NEURAL ACTIVITY DURING A SIMPLE REACHING TASK IN MACAQUES IS COUNTER TO GATING AND REBOUND IN BASAL GANGLIA-THALAMIC COMMUNICATION

Bettina C. Schwab[1,2], Daisuke Kase[3,4], Andrew Zimnik[5], Robert Rosenbaum[6], Marcello G. Codianni[7], Jonathan E. Rubin[4,7], Robert S. Turner[3,4*]

[1] Department of Neurophysiology and Pathophysiology, University Medical Center Hamburg-Eppendorf, Hamburg, Germany, [2] Technical Medical Center, University of Twente, Enschede, Netherlands, [3] Department of Neurobiology, University of Pittsburgh, Pittsburgh, Pennsylvania, USA [4] Center for the Neural Basis of Cognition, University of Pittsburgh, Pittsburgh, Pennsylvania, USA [5] Department of Neuroscience, Columbia University Medical Center, New York, New York, USA [6] Department of Applied and Computational Mathematics and Statistics, University of Notre Dame, South Bend, Indiana, USA [7] Department of Mathematics, University of Pittsburgh, Pittsburgh, Pennsylvania, USA.

***Address correspondence to:**

Robert S Turner, PhD
Department of Neurobiology
University of Pittsburgh
4047 BST-3, 3501 Fifth Avenue
Pittsburgh, PA 15261
Phone: 412-383-5395
Fax: 412-383-9061
email: rturner@pitt.edu

Abstract	200 words
Introduction	996 words
Discussion	3,010 words
Total	20,704 words
References	106
Tables	3
Figures	6 + 14

Short title: Basal ganglia-thalamic communication

Keywords: Basal ganglia; Reaching; Non-human primate; Gating hypothesis; Internal globus pallidus; Ventrolateral thalamus; Movement control

Funding: This work was supported by the National Institute of Neurological Disorders and Stroke at the National Institutes of Health grant numbers R01NS091853, R01NS113817 (to RST) and R01NS070865 (to RST and JER), NSF awards DMS1516288 and DMS1724240 (to JER), the Center for Neuroscience Research in Non-human primates (CNRN), 1P30NS076405-01A1, NSF awards DMS-1654268 and Neuronex DBI-1707400 (to RR), and the Netherlands Organization for Scientific Research (NWO, NDNS+ grant 613.009.012). The funders had no role in study design, data collection and analysis, decision to publish, or preparation of the manuscript.

Acknowledgements: We thank Lisa Nieman-Vento and Patrick Rice for their contributions to animal care.

Abstract

Task-related activity in the ventral thalamus, a major target of basal ganglia output, is often assumed to be permitted or triggered by changes in basal ganglia activity through gating- or rebound-like mechanisms. To test those hypotheses, we sampled single-unit activity from connected basal ganglia output and thalamic nuclei (globus pallidus-internus, GPi, and ventrolateral-anterior nucleus, VLa) in monkeys performing a reaching task. Rate increases were the most common peri-movement change in both nuclei. Moreover, peri-movement changes generally began earlier in VLa than in GPi. Simultaneously-recorded GPi-VLa pairs rarely showed short-timescale spike-to-spike correlations or slow across-trials covariations and both were equally positive and negative. Finally, spontaneous GPi bursts and pauses were both followed by small, slow reductions in VLa rate. These results appear incompatible with standard gating and rebound models. Still, gating or rebound may be possible in other physiological situations: Simulations show how GPi-VLa communication can scale with GPi synchrony and GPi-to-VLa convergence, illuminating how synchrony of basal ganglia output during motor learning or in pathological conditions may render this pathway effective. Thus, in the healthy state, basal ganglia-thalamic communication during learned movement is more subtle than expected, with changes in firing rates possibly being dominated by a common external source.

Introduction

The connection between the basal ganglia (BG) and one of its major downstream targets, the thalamus, has received increased attention recently [1; 2; 3; 4; 5] due to its role as a key pathway by which the BG can influence cortical function. It is well established that the BG-thalamic projection is composed of GABAergic neurons [6; 7; 8] that fire at high tonic rates of about 60 spikes/sec in non-human primates at rest [9] and that this projection terminates densely on thalamocortical relay neurons, as well as on GABAergic thalamic interneurons (in species in which these exist) [10; 11]. The fundamental mechanism by which the BG-thalamic pathway communicates task-related information, however, remains uncertain [2]. A long-standing and widely accepted theory states that pauses in BG output activity "gate" the task-related activation of thalamus via disinhibition [12; 13; 14; 15; 16; 17]. More specifically, the high tonic firing rate of BG output neurons normally prevents thalamic neurons from responding to excitatory inputs (e.g., from cortex), but a task-related pause in BG output, which typically extends over one hundred milliseconds or more, would act as a disinhibitory opening of the gate allowing a temporally-coordinated task-related activation of thalamus. A competing theory hypothesizes that BG output may promote subsequent thalamic activation. Specifically, the low threshold spike (LTS) mechanism common to thalamocortical neurons [4; 18; 19; 20] may produce rebound bursts of thalamic activity following a cessation of transiently elevated inhibition from the BG (e.g., following task-related increases in BG output activity) [4, 22]. Both of these theories predict a tight temporal control of thalamic task-related responses by changes in BG output; more specifically, the latency of task-related changes in BG output activity should lead by a short time interval the resulting responses in thalamus. The gating hypothesis, in addition, predicts an inverse relationship in the signs of task-related changes in BG and BG-recipient

thalamus, with the incidence (i.e., relative frequency of occurrence) of task-related increases in BG output associated with a proportional incidence of decreases in activity in BG-recipient thalamus.

Others have suggested that the influence of BG output on thalamus is more subtle, primarily consisting of a modulation of thalamic activity, while cortex is the primary driver. This idea arose initially from the observation that inactivations within the output nucleus of the BG did not abolish task-related activity in the BG-recipient thalamus [23; 24]. That result was corroborated recently by Goldberg and Fee [25] using the songbird model. Goldberg and Fee [25] also substantiated two insights suggested previously from between-studies comparisons [26; 27]: first, that task-related increases in firing are far more prevalent than decreases both in BG-output neurons [28; 29; 30; 31; 32] and in BG-recipient thalamus [17; 33; 34]; and second, that the latencies of task-related activity in BG output neurons [28; 31; 32] do not lead those of the BG-recipient thalamus, but may in fact lag behind them [17; 33; 34]. Goldberg and Fee [25] did observe strong inhibitory effects of individual BG efferents onto thalamic neurons. In that study, the primary mode of BG-thalamic communication was an entrainment of thalamic spiking to the interspike intervals of BG efferents. A similar mechanism, if present in mammals, would provide a way for BG output to modulate the timing of thalamic spiking without requiring, as the gating and rebound models do, strict relationships in the timing and sign of task-related changes in firing. However, the high strength of the entrainment observed by Goldberg and Fee [25] is likely a product of the unique synaptic anatomy of this circuit in the songbird [35] that is not present in mammals [10; 36].

The BG-thalamic loop circuit devoted to skeletomotor function provides a well-defined anatomically-segregated substrate for testing the theories outlined above. This circuit receives

convergent input from motor and somatosensory cortical areas and projects back to the motor cortices by way of a monosynaptic projection from the internal globus pallidus (GPi) to the anterior ventrolateral thalamus (VLa) [37; 38]. Experimentally-induced perturbations of this circuit are known to impair the vigor, timing and initiation of voluntary movement [27; 39; 40]. A substantial diversity of opinion remains, however, about the specific contributions that this circuit makes to motor control under normal physiologic conditions [37; 41; 42; 43; 44; 45]. A better understanding of the mechanisms that govern GPi-to-VLa communication is likely to reduce that uncertainty. Other downstream targets of the BG, including areas of the brainstem and midbrain [46; 47], are also of great importance but are not investigated here.

Here, for the first time in non-human primates (NHPs), we studied single-unit activity sampled simultaneously from connected regions of GPi and VLa while animals performed a highly standardized reaching task. Contrary to predictions of the gating theory, movement-related increases in discharge were common in both GPi and VLa. Furthermore, VLa task-related changes tended to begin earlier than GPi changes, inconsistent with ideas of gating and rebound. The firing of simultaneously recorded cell pairs in GPi and VLa was weakly (if at all) correlated, in contrast to what would be expected from gating or rebound models; bursts and pauses in GPi spontaneous activity had similar weak effects on VLa firing. Hence, our results challenge the view that task-related activity in the BG-recipient thalamus arises under most or all conditions from gating or rebound-inducing signals transmitted from the BG. We use simulations to show how the strength of GPi-VLa communication can depend critically on the degree of anatomical convergence in the GPi-VLa circuit and the strength of spike synchrony within GPi. Thus, our results do not speak to the function of this pathway under other task conditions or behavioral states and, in fact, are in congruence with existing observations of effective thalamic inhibition

by synchronized BG output. Our results suggest that, during performance of well-learned tasks in neurologically-normal animals, temporal influences of GPi outputs on VLa activity are subtle and at most modulatory. Control over the timing and intensity of both pallidal and thalamic discharge may be dominated by other, possibly cortical, inputs.

Results

Basic approach, database, and activity at rest

We studied the single-unit activity of neurons sampled from connected regions of the GPi and VLa. The spiking activity of isolated single-units was recorded from both areas simultaneously in macaque monkeys while the animals performed a two-choice reaction time reaching task for food reward [48; 49]. In short, animals were trained to hold their left hand at a home position located immediately to the left of the animal at waist height. Two visual targets were located 14 cm apart at shoulder height on a vertically-mounted response panel positioned 30 cm in front of the animal. After a randomized home position hold period, one of the targets (chosen pseudo-randomly trial-to-trial) was lit and the animal had to move the left hand swiftly to that target (distance: ~37 cm) and then hold there to obtain a reward. The right arm was restrained in a padded splint throughout a data collection session. Multiple microelectrodes or 16-contact linear probes were positioned acutely in the arm-related regions of both nuclei [50].

We used a combination of electrophysiologic techniques to ensure that recordings were obtained from anatomically connected regions of GPi and VLa. Consistent with previous observations [34; 51] the location of the VLa nucleus was distinguished from surrounding thalamic regions – and from the cerebellar-recipient posterior ventrolateral nucleus (VLp) in particular – by the

presence of a short-latency inhibition of spiking in response to electrical stimulation of the GPi and the absence of short-latency excitation in response to stimulation of the superior cerebellar peduncle (SCP, Fig. 1B). This electrophysiologic localization of the VLa/VLp border was performed during initial mapping studies prior to formal data collection. Across multiple parallel electrode tracks, thalamic neurons inhibited by GPi stimulation (*yellow* tick marks in Fig. 1A, examples 1 and 2 in Fig. 1B) were always encountered at locations that were dorsal and anterior to neurons excited by SCP stimulation (*green* tick marks in Fig. 1A, example 4 in Fig. 1B). In most cases a narrow border (<0.5mm) separated the deepest GPi-inhibited neuron and the dorsal-most SCP-excited cell (Fig. 1A) and the location of this border aligned closely across adjacent electrode tracks. Coincident inhibition from GPi stimulation and excitation from SCP (e.g., Fig. 1B3) was observed only at a small number of thalamic locations and those were located exclusively in the narrow border between GPi-inhibited and SCP-excited regions (*red* tick mark in Fig. 1A, example 3 in Fig. 1B).

The sub-regions of GPi and VLa that compose the arm-related BG-thalamic circuit were identified by testing for short-latency effects of electrical stimulation in arm-related areas of primary motor cortex (Fig. 1C). Previous studies have shown that stimulation of cortex can elicit complex triphasic responses in GPi neurons, via two- and three-synapse arcs through the BG [51; 52] (Fig. 1C *top*), and that excitation of corticothalamic projections can elicit excitatory and inhibitory responses in VLa neurons [53] (Fig. 1C *bottom*).

During subsequent data collection, thalamic single-units were included in the database as VLa units if the electrode contact was located below the reticular nucleus of the thalamus (which is easily recognized neurophysiologically), above the VLa/VLp border (as defined above), and within 0.5mm of a neuron affected by M1 stimulation. Single-units sampled from the GPi were

included if they were located in the dorsolateral portion of the nucleus and were encountered within 0.5mm of a neuron affected by M1 stimulation. (See Supporting Information S1 for anatomic locations of all included single units relative to observed electrophysiologic landmarks and inferred nuclear borders.)

Insert Figure 1 around here

A-B. Exemplar results from microelectrode mapping in the vicinity of the VLa thalamus. Single-units encountered along parallel electrode trajectories were classified as being located in striatum (light gray tick marks), reticular nucleus of the thalamus (dark gray) or the VL thalamus. Neurons in VL thalamus were further classified as VLa neurons if they were inhibited by stimulation of the GPi and not excited by stimulation of SCP (yellow tick marks). Fig. 1B1-2 shows overlaid peri-stimulus raw waveforms (left) and raster plots of sorted spikes (right) from two example locations in VLa (locations 1 and 2 in Figs. 1A and B) at which GPi stimulation evoked a pause in neuronal activity and SCP stimulation had no effect. Neurons in VL were classified as VLp neurons if they were excited by stimulation of SCP and did not respond to stimulation of the GPi (green tick marks in Fig. 1A; e.g., location 4 in Figs. 1A and B). Neurons located at the border between VLa and VLp occasionally responded to stimulation of both GPi and SCP (red tick mark, location 3 in Figs. 1A and B). Neurons that did not respond to stimulation were classified as VLa neurons (black tick marks Fig. 1A) only if they were located antero-dorsal to the VLa/VLp boundary and postero-ventral to the reticular nucleus of the thalamus.

C. Regions of the GPi and VLa that belong to the arm-related BG-thalamic circuit were identified by testing for short-latency effects of electrical stimulation in arm-related areas of primary motor cortex. GPi neurons were included if sampled from regions at which stimulation of motor cortex (time zero) evoked a triphasic response at short latency (top, raster plot of sorted spikes). VLa neurons were included if sampled from regions at which stimulation of motor cortex evoked a pause or burst of activity at short latency (middle and bottom panels, respectively).

For analyses of task-related changes in activity, a total of 209 single-units met the criteria to be included as GPi neurons and 218 as VLa neurons (Table 1). These units were studied over the course of 126±82 trials of the behavioral task (mean ±SD; mean 63 trials for each of two movement directions; minimum number of trials per direction: 16; minimum duration of recording: 174.7 s). As expected, the resting firing rate of GPi neurons was significantly higher

than that of VLa neurons (Table 1; $p=1\times10^{-81}$, rank sum test) [34], and those rates and the differences between neural populations were highly consistent for the two animals (Table 1; p=1, rank sum test). Also, as expected, the action potentials of GPi neurons were short in duration as compared with those of VLa neurons (Table 1; $p=1\times10^{-33}$, rank sum test).

The mean firing rate of most single-units showed small but significant ramps during the start position hold period (i.e., before presentation of the task's go cue; $p<0.05$, linear regression; 97% and 98% of GPi and VLa cells, respectively). This phenomenon is illustrated for exemplar GPi and VLa units in Fig. 2A. The GPi unit's firing rate increased slowly (4.3 spikes/s^2, $p<0.001$) during the ~1.2 s hold period before appearance of the go cue (*red tick marks* in rasters, Fig. 2A) while that of the VLa unit decreased slowly (-6.7 spikes/s^2, $p<0.001$; Fig. 2A). For both GPi and VLa unit populations, the observed slopes were distributed symmetrically around zero (means: −0.05 and −0.14 spikes/s^2 respectively; p=0.29, rank sum test). Positively- and negatively-sloped ramps in activity were equally common (49% and 51%, respectively) and those fractions did not differ significantly between GPi and VLa neurons or directions of movement ($p>0.27$, chi-square test). These linear trends in delay period activity were taken into account by the algorithm used to detect peri-movement changes in firing rate, as described below.

Task performance

Both animals performed the behavioral task in a highly stereotyped fashion with short reaction times and movement durations (Supporting Information S2). Reaction times did not differ significantly between the two animals [$F(1,452)=0$, p=0.97, ANOVA] or between the two reach directions [$F(1,452)=0.2$, p=0.68]. There was a slight (7 msec), yet significant, difference

between the two animals in the effect of target direction on reaction times [animal × direction interaction; $F(1,452)=9.6$, $p=0.002$]. Movement durations were longer for reaches to the more-distant, right target than to the left [$F(1,453)=416$, $p=4\times10^{-66}$]. NHP G moved more slowly overall compared with NHP I [$F(1,453)=1419$, $p=1\times10^{-141}$] and that slowing was more dramatic for the right target [animal × direction interaction; $F(1,452)=36.3$, $p=1\times10^{-9}$]. Errors and outliers in task performance occurred at low rates in both animals [4.8±1.2% and 3.4±0.7% of trials in animals G and I, respectively; mean ± standard error of the mean (SEM)]. Reach-related modulations in muscle activity (measured by electromyography, EMG, sampled during a subset of data collection sessions) were highly stereotyped across trials (Supporting Information S3). Importantly, reach-related changes in agonist muscle EMG began well before the overt onset of movement as detected mechanically and those onset latencies were similar for the two animals (-123 and -135 ms in NHP G and I, respectively; Supporting Information S3). The movement-related modulations in EMG differed quantitatively for the two directions of movement (widths of traces reflect SEMs in Supporting Information S3) but not in sign. The implications of these EMG results for the interpretation of single unit activity are discussed below.

Movement-related increases in firing are common in both GPi and VLa

We examined the peri-movement activity of neurons in GPi and VLa to test for evidence of an inverse relationship in their rate changes, as predicted by the gating hypothesis. In these analyses, responses for each direction of movement were considered separately. Large proportions of both neural populations modulated their firing rates around the onset of reaches to the left or right target (Table 1). We constructed mean spike-density and interspike-interval functions for each single-unit separately for movements to left and right targets and then tested

for significant changes in firing rate relative to that unit's baseline activity [i.e., linear trend ±confidence interval (CI) of activity prior to go-cue presentation, *yellow sloped lines* in Fig. 2A and Supporting Information S4]. To avoid a bias inherent to spike density functions toward detecting rate increases relative to rate decreases, we tested for peri-movement decreases in firing as increases in the mean interspike-interval. (See Supporting Information S4 for examples. See *Materials and methods* and Supporting Information S5 for a simulation-based test for biases in the response detection algorithm used.) Figure 2A shows examples of the activity observed in individual GPi and VLa units. The GPi single-unit showed a polyphasic change in firing that began with an increase in firing at −93 ms followed by a large decrease beginning at +77 ms relative to movement onset (*yellow and blue vertical lines, respectively*). The VLa single-unit showed a monophasic increase in firing that first reached significance at −115 ms relative to movement onset. (The subsequent small but long-lasting depression in rate during movement did not reach significance.) Nearly all single-units showed a significant peri-movement change in discharge for at least one direction of movement, with slightly fewer VLa units responding (99% of GPi neurons and 94% of VLa neurons; p=0.02, chi-square test).

Insert Figure 2 around here

A. Activity of one exemplar single-unit sampled from GPi (left) and from VLa (right) aligned to the time of movement onset (vertical black dashed line). Peri-movement spike-density functions (top) and rasters (bottom) show highly consistent changes in discharge rate around the time of movement onset (time zero). Vertical yellow and blue lines: the times of onset of increases and decreases in discharge detected relative to that unit's baseline activity (sloping yellow trend line ±confidence interval). For raster plots, trials are sorted according to reaction time. Red tick marks: trial-by-trial times of go-cue presentation.

B. Spike-density functions of all single-units studied sorted according to response form and response onset latency (earliest onsets at the top for each response form). Spike density functions were z-scored relative to mean rate prior to go-cue presentation and displayed on a color scale.

C. Population averaged spike-density functions for all GPi and VLa units (black) and for sub-populations with different response forms (as labeled). Shaded areas above/below the means reflect the SEM across units.

Data and code to reproduce this figure can be found in https://doi.org/10.5061/dryad.0cfxpnvxm (Fig2_3_S8_S9.m).

The form and timing of neuronal responses differed widely between neurons (see Fig. 2B and Supporting Information S4) and, occasionally, between directions of movement (see below). First, we considered neuronal responses independently for each movement direction and tested for differences between GPi and VLa populations in the incidence of different forms of peri-movement activity (see Table 1 and Fig. 2B). Monophasic changes in firing (composed of a simple increase or decrease in firing) were the most common change detected in both GPi and VLa, amounting to 66.7% and 88.9% of all responses detected, respectively. Monophasic responses were more common in VLa than in GPi ($p=2.8\times10^{-12}$, chi-square test). Conversely, polyphasic responses – a series of one or more increase *and* decrease in firing – were more common in GPi than in VLa. Individual single-unit examples of each type of response are shown in Supporting Information S4 and all detected responses are shown sorted by response type and latency in Fig. 2B.

Monophasic increases were the most common form of response both in GPi and in VLa (48.7% and 65.3% of responses detected, respectively; Table 1). When the individual phases of all detected responses were considered independently, increases in firing were also more common than decreases both in GPi and in VLa (61.5% and 68.8% of changes, respectively; $p=1.2\times10^{-17}$, chi-square test) with increases being nominally more common in VLa than in GPi ($p=0.03$, chi-square test). Simulations indicated that the observed high incidence of increases in both GPi and

VLa was unlikely to be the byproduct of methodologic biases toward the detection of increases (see Supporting Information S5 and *Materials and methods*).

Another way to compare the balance of task-related increases and decreases between GPi and VLa is to examine the mean firing rate across the two populations. Population averages combined across all responses types (*All* in Fig. 2C) showed increases in firing rate during the peri-movement period for both cell types. This inclination toward increases was confirmed quantitatively by integrating changes in firing rate from baseline across the peri-movement epoch individually for each neuron. The mean of this integrated change was positive both for GPi and VLa ($z=7.37$, $p=1.7\times10^{-13}$, and $z=6.59$, $p=4.7\times10^{-11}$ for GPi and VLa, respectively, rank sum test; Table 1).

The observations outlined above were confirmed in analyses that considered potential influences of the direction of movement on unit discharge. While the majority of GPi neurons (109 out of 206) and some VLa neurons (56 out of 179) showed significantly stronger responses to one of the movement directions, movement direction did not affect the magnitude or timing of peri-movement activity across whole GPi and VLa populations (Supporting Information S6 A; $z<1.76$, $p>0.07$, and $z<1.0$, $p>0.35$ for GPi and VLa, respectively, rank sum tests performed separately for each timepoint, uncorrected for multiple comparisons). The form of an individual neuron's peri-movement response (increase, decrease, or polyphasic) was typically consistent for reaches to the left and right targets (Supporting Information S6 B). This was true for both GPi neurons and VLa neurons (71% and 78% of neurons, respectively; shown by the color of bins along the matrix diagonals in Supporting Information S6 B; $p<10^{-16}$, chi-square test for homogeneity computed separately for GPi and VLa distributions). Again, increases were more common than decreases and polyphasic changes were more common in GPi than in VLa

populations (compare diagonals between matrices for GPi and VLa in Supporting Information S6 B; $p=2.9\times10^{-6}$, chi-square test). We found no evidence for directional biases in the incidence of different forms of responses (e.g., decreases were not more common for one direction of movement over the other). A comparison of integrated changes in firing rate further reinforced these conclusions. For both GPi and VLa populations, the polarity and magnitude of a neuron's integrated change in firing for leftward movements was correlated with its change for rightward movements (Supporting Information S6 C; $r>0.6$, $p<1\times10^{-25}$ for both GPi and VLa populations). Notably, few points fell in the upper left and lower right quadrants of Supporting Information S6 C reflecting the fact that few neurons were modulated reciprocally by the two movement directions or exclusively for one direction. Simple conceptions of the gating model predict that such relations with movement direction would be common in GPi. The polarities of integrated changes (i.e., increase versus decrease from baseline rate) and the degree to which polarities agreed between movement directions were distributed very similarly for GPi and VLa populations (Supporting Information S6 D; $p=0.68$, chi-square test). However, despite this general similarity of individual units' responses for left and right reaches, peri-movement activity did differ significantly between left and right reaches for substantial fractions of GPi and VLa neurons (53% and 31% of units, respectively; Supporting Information S6 C; $p<0.005$, rank sum test).

In summary, the general distribution of different response types and the predominance of firing-rate increases were similar in GPi and VLa (see Supporting Information S6 E), contrary to the prediction from the gating hypothesis that this relationship would be reciprocal. There was general similarity in the form and the sign of responses detected in GPi and VLa with the most

notable difference between populations being that polyphasic responses were more common in GPi than in VLa.

Response onset latencies in GPi and VLa are incompatible with gating and rebound

The gating theory predicts that decreases in GPi activity should precede and permit increases in VLa firing, while a rebound mechanism would also feature changes in GPi activity that precede those in VLa. To address these predictions, we compared the times of onset for all individual changes in firing detected in GPi and VLa single units. As is evident in both Fig. 2B and Fig. 3A, response onset times were distributed widely across the peri-movement period and that was equally true for neural responses in GPi and VLa. Quantitative comparison, however, showed that, on average, GPi changes in discharge began later than those in VLa (median onset times: −47 and −90 ms for GPi and VLa populations, respectively; $z=3.31$, $p=2.4\times10^{-5}$, rank sum test; Fig. 3A), in contrast to the relationship posited in the gating and rebound frameworks. The more specific gating prediction states that decreases in GPi activity should precede VLa increases and, similarly, GPi increases precede VLa decreases. In contradiction, the distribution of GPi decreases lagged in time behind that of VLa increases (median onset times: −27 and −88 ms for GPi and VLa populations, respectively; $z=3.19$, $p=4.9\times10^{-4}$, rank sum test; Fig. 3B). Similarly, VLa decreases did not follow but rather preceded GPi increases (median onset times: −62 and −108 ms for GPi and VLa populations, respectively; $z=2.58$, $p=0.01$, rank sum test; Fig. 3C). Although the overall difference in distributions for GPi and VLa response latencies is inconsistent with the gating hypothesis, the latency distributions do overlap substantially (Fig. 3) leaving the possibility that a subpopulation of early-onset GPi responses begin earlier than later-onset VLa responses and thus could contribute to their generation (or engage in “gating”). To

estimate how common such cases might be, we compared the timing and sign of every individual response detected in the whole database of GPi units against every response detected in the VLa database (regardless of whether or not GPi and VLa units were recorded from simultaneously) and computed the fraction of comparisons that conflicted with the gating hypothesis with respect to the mentioned parameters. A large preponderance of these comparisons (96%, n = 178,846 of 187,154 comparisons) directly conflicted with the gating hypothesis due to the relative timing or signs of the responses (i.e., GPi onset precedes VLa onset by 0 – 50 msec and response signs are opposite). Thus, when the apparent large overlap in latency distributions illustrated in Fig. 3 is additionally constrained by predictions regarding response signs the possibility for a gating-like latency relationship was found in only 4% of all possible GPi-VLa neuron pairs. The potential presence of an early-onset GPi subpopulation is addressed in more detail in the next sections. The latency distributions described here did not differ significantly between the two directions of movement for neurons in either GPi or VLa ($z<1.19$, $p>0.08$, rank sum test). In addition, the latency estimation algorithms used here showed only slight non-significant biases when applied to simulated neuronal responses that matched the metrics of real GPi and VLa neuronal responses ($z<0.19$, $p>0.2$, rank sum test; Supporting Information S7; see *Materials and methods*). Moreover, the small biases observed in the simulation results were toward *longer* lags for the detection of VLa responses relative to the detection of GPi responses – the converse of what was observed in the empirical latency results. Qualitatively similar results to those from the general comparison of latencies (Fig. 3) were also found when the latency analysis was restricted to the preferred direction of single units with peri-movement activity that was significantly directional (Supporting Information S8 A-C).

Insert Figure 3 around here

*A. Cumulative distributions of onset latencies of all significant peri-movement changes in firing detected in GPi neurons (blue) and VLa neurons (purple). Responses in VLa precede responses in GPi by a median of 43ms. (** $p=2.4\times10^{-5}$ rank sum test)*

*B. Response onset latencies of VLa increases (purple) lead GPi decreases (blue) by a median of 61ms. (** $p=4.9\times10^{-4}$ rank sum test)*

*C. Response onset latencies of VLa decreases (purple) lead GPi increases (blue) by a median of 46ms. (** p=0.01 rank sum test)*

Data and code to reproduce this figure can be found in https://doi.org/10.5061/dryad.0cfxpnvxm (Fig2_3_S8_S9.m).

As a further step to control for potential biases in latency estimation due, e.g., to differences between GPi and VLa populations in baseline firing rate and rate variability, we re-estimated response onset latencies using an alternate approach based on the time at which an activity function crosses a fraction of the peak change (see *Materials and methods*). That approach resulted in slightly earlier onset latencies overall (median latency shift: -14 ms), but the differences in latencies between GPi and VLa populations were fully consistent with those described above for the standard analysis (see Supporting Information S8 D-F). Thus, to summarize, the timing of changes in peri-movement discharge is not consistent with the idea that GPi activity triggers or gates task-related activity in VLa.

Finally, we looked for evidence that a subpopulation of early onset GPi responses might lead and thereby gate subsequent VLa responses. For example, one might predict from the gating hypothesis that the magnitude of a GPi response is associated closely with the size of the response that it evokes milliseconds thereafter in VLa. Thus, GPi and VLa populations should show similar relationships between response magnitude and response latency if any such

relationship existed. We therefore tested for relationships between response magnitude (measured here as mean change from baseline firing rate) and latency for all increases and decreases detected in GPi and VLa (Supporting Information S9). Contrary to predictions, however, the observed relationships differed markedly between GPi and VLa. In VLa, early latency responses were larger in magnitude than late onset responses as evidenced by the presence of significant negative correlations between latency and magnitude for both increase- and decrease-type VLa responses (Spearman $p<0.05$) and significant 1-way ANOVAs across latency quartiles [$F(3,248)=4.3$, $p=0.005$ and $F(3,112)=4.3$, $p=1\times10^{-7}$, respectively]. In GPi, however, no such relationship was found for increase-type responses [Spearman $p=0.95$; $F(3,308)=1.5$, $p=0.2$] and nominally the opposite was found for decrease-type responses [Spearman $p=0.65$; $F(3,198)=3.0$, $p=0.03$]. In sum, the relation of response magnitudes and latencies does not support rebound- or gating-like mechanisms.

We next investigated the possibility that GPi to VLa communication might be evident in the activity of cell pairs sampled simultaneously from the two structures.

Correlated activity in GPi-VLa cell pairs is rare and unbiased

Both gating and rebound triggering of thalamic activity by the BG should produce strong correlations in the precise timing of spikes in GPi and VLa. Contrary to that expectation, we found little evidence for strong short time-scale spike-to-spike interactions between GPi and VLa unit pairs (Fig. 4 A-F). When we computed cross-correlation functions (CCFs) for pairs of spike trains sampled simultaneously from GPi and VLa, only 3.5% of the CCFs showed any statistically significant modulation (15 of 427 cell pairs; $p<0.05$ relative to a 20 ms jittered control; Table 2). Similarly, small fractions of CCFs reached significance when the analysis was

restricted to a rest period during the start-position hold period (2.2% of pairs; 4 out of 183), or to the peri-movement period (5.2% of pairs; 9 of 172; Table 2). For the movement period, the fraction of significant correlations did not increase when correlations were computed separately for the two movement directions (4.1% of pairs; 14 out of 342) and there was no evidence that the occurrence of significant correlations was greater for one direction of movement over the other (6 out of 171 vs 8 out of 171; p=0.59, chi-square test). (Note that the number of pairs differs between time periods considered due to the strict selection criteria used to ensure adequate statistical power, as described in more detail in *Materials and methods.* The lower incidence of significant correlations in the direction-specific analysis may be related to the reduced number of trials.) Furthermore, the overall distribution of the peak absolute correlation values was not greater than the distribution of control peak absolute correlations taken from CCFs generated after jittering spike times within 20 ms time windows (Fig. 4 A-C, uncorrected p-values: 0.975 for whole recordings, 0.675 for rest, and 0.998 for movement periods; one-sided permutation test). For none of the time periods considered did the rate of occurrence of significant correlations exceed by a significant degree the 5% rate of false-positives detected in the control distributions. More broadly, population averages of the CCFs did not extend beyond the confidence intervals from the control data (Fig. 4 D-F, p>0.05 relative to shuffled control).

Among the small number of individual CCFs that did exceed the threshold for significance, none showed features consistent with being the product of strong monosynaptic GPi-to-VLa inhibition. Contrary to the expectation that GPi-to-VLa CCF effects would be predominantly inhibitory (i.e., negative), roughly equal numbers of the CCF peaks detected as significant were positive and negative (8 versus 7, respectively; p=0.79, chi-square test; Supporting Information S10 D-F). Only two CCFs showed a long-lasting (>5 msec) reduction in

VLa firing following the GPi spike (Supporting Information S10 D, first and third examples). Those two effects showed features consistent with a slow rhythmic GPi-VLa synchronization at 25 Hz (~40 ms cycle length). Slow rhythmic synchronizations at frequencies <25 Hz were also present in some individual raw CCFs, but those effects were removed implicitly by subtracting the average jitter control CCF (see *Materials and methods*). The magnitude of individual CCF peaks correlated closely with the width of the CCF's 95% confidence interval (whole recordings: $r=0.82$, $p<10^{-10}$; during rest: $r=0.62$, $p<10^{-10}$; during movement: $r=0.61$, $p<10^{-10}$), which reflects how noisy the estimate of the CCF was (Supporting Information S10 G-I). In other words, the narrower the 95% confidence interval the smaller the estimation noise and, incidentally, the smaller the detected CCF peak. This was true even for CCF peaks that were detected as significant (red X's in Supporting Information S10 G-I), thus reinforcing the view that the CCF peaks detected here as significant may in fact have been false-positive noise events. Together, these observations suggest that short time-scale spike-to-spike interactions between GPi and VLa unit pairs, if present, were too small and/or too uncommon to be detected with the methods used here.

Given these results, it was important to consider the sensitivity of our methods. To that end, we estimated how small of a known, experimenter-imposed, spike-to-spike correlation could be detected reliably in simulated spike-train pairs that matched the firing rates and recording durations of each empirical GPi-VLa pair. We also computed the upper bounds to each measured correlation (see *Materials and methods* for details). [These two measures were distributed very similarly within each analysis time period (whole recordings, rest, or movement; Supporting Information S11 D-F).] Not surprisingly, the minimum reliably detectable correlation (our measure of sensitivity) varied across the population of simulated pairs due to

between-pairs differences in firing rates and duration of data collection. This led to a trade-off between the number of pairs considered and the within-pair sensitivity for detection of small correlations. Considering whole recordings, it was possible to detect correlations smaller than 20.1% of baseline rate in 90% of pairs (n=388), and correlations smaller than 10.5% in 50% of pairs (n=216) (Supporting Information S11 A). In the most sensitive 10% of pairs, it was possible to detect simulated correlations smaller than 6.1% of baseline. Even in this last subset in which real correlations should have been most easily detected, the number and magnitude of empirically-detected CCF peaks did not exceed what would be expected if the CCFs were composed of noise alone. Analyses applied to rest and movement epochs lead to similar conclusions (Supporting Information S11 B-C). Again, the magnitude of individual CCF peaks correlated closely with the minimum reliably detectable correlation (whole recordings: $r=0.98$, $p<10^{-10}$; during rest: $r=0.97$, $p<10^{-9}$; during movement: $r=0.98$, $p<10^{-10}$), reflecting the noise in CCF estimation (Supporting Information S11 D-F), for all as well as for significant CCFs (red X's).

In sum, short latency cell-to-cell interactions were too small and/or too uncommon to be detected reliably using the approach applied here. These observations bring into question not only the standard gating and rebound hypotheses, but also more fundamental assumptions about the mechanisms at play in GPi-VLa communication. We addressed this issue in more depth using a computational approach (see *Simulations…* section, below).

Next, we tested for slow trial-to-trial correlations in firing rate ('noise correlations') between simultaneously-recorded GPi-VLa cell pairs. This analysis was performed separately for rest and peri-movement periods. If gating was a common mechanism in GPi-VLa communication, then the majority of significant noise correlations would be expected to be negative whereas some

versions of the rebound mechanism predict more frequent positive correlations due to the capacity of brief increases in GPi activity to effectively recruit prolonged rebound-supporting currents in VLa [4; 18; 19; 20]. We found that the overall distribution of noise correlations was not significantly different from the control distribution (Fig. 4 G-H; p=0.07 during rest, p=0.388 during movement; permutation test). Nevertheless, noise correlations did reach significance during rest for 5.4% of cell pairs (18 of 332 pairs; $p<0.05$ relative to shuffled controls; Table 2) and during movement for 7.2% of cell pairs (27 of 372 pairs). Roughly equal fractions of those significant correlations were positive (*orange* lines, Fig. 4 G-H) and negative (*magenta* lines; 44% versus 56% during rest and 41% versus 59% during movement, respectively; Table 2). Also between the recorded GPi neurons, cross-correlations and noise correlations were low (see Supporting Information S12). Examples of the largest three GPi-VLa noise correlations during movement are shown in Supporting Information S13. There was no evidence that the significant effects showed a bias in prevalence toward positive or negative correlations (p=0.64 during rest, p=0.34 during movement; chi-square test).

Thus, neither of the tests for correlated activity in GPi-VLa cell pairs yielded evidence consistent with the gating or rebound hypotheses.

Insert Figure 4 around here

Absence of fast correlations between GPi and VLa spikes. A-C: Histograms of peak absolute CCF values between GPi and VLa units (black) for whole recordings (A), during rest (B) and during movement (C). Jitter control distributions (20ms jitter intervals) are shown in gray. D-F: Population average CCFs (black) and 95% confidence intervals (gray) based on the jitter control. G-H: Low noise correlations between GPi and VLa during both rest (G) and movement (H). Noise correlations exceeding the 95% confidence limits are shown in orange (positive) and magenta (negative). Dashed vertical lines indicate the medians of the distributions. For both rest and movement, test distributions did not differ significantly from the control distribution (gray). No significant bias towards positive or negative correlations was found.

Data and code to reproduce this figure can be found in https://doi.org/10.5061/dryad.0cfxpnvxm (Fig4_S10to13.m).

VLa activity decreases with bursts and pauses in GPi activity

Bursts and pauses are common features of GPi activity that could facilitate the transmission of information to VLa. The post-synaptic effects in VLa of GPi bursts and pauses could also be larger in magnitude and easier to detect than effects produced by single GPi spikes. We therefore estimated the influences of bursts and pauses in GPi unit activity on the firing rate of VLa neurons during the rest period (Fig. 5). The gating hypothesis predicts that GPi bursts should be associated closely in time with reductions in VLa firing rate and GPi pauses with VLa increases. The rebound hypothesis predicts that GPi burst offsets should be followed by increases in VLa firing. We detected the occurrences of bursts and pauses in each GPi unit's rest period activity separately using standard methods [54] and then averaged the firing rates of simultaneously-recorded VLa neurons around the times of GPi burst onset, burst offset, and pause onset. The resulting burst-triggered, burst offset-triggered, and pause-triggered averages of VLa activity were averaged across the populations of qualifying GPi-VLa pairs (Fig. 5 A-C; Table 2; see *Materials and methods* for selection criteria and Supporting Information S14 for an example GPi burst offset-triggered average VLa firing rate from one pair). Small but significant transient decreases in VLa population spike rate were evident following both the onsets and offsets of bursts. That decrease began at a longer lag following the onset of bursts (119 ms) than after their offsets (95 ms) with the difference (24 ms) equal to the observed mean duration of GPi bursts (24 ms). The presence of a decrease in VLa firing rate following the offset of GPi bursts is not consistent with the predictions of either gating or rebound hypotheses.

Surprisingly, a deceleration in VLa activity was also associated with pauses in GPi activity (Fig. 5 C). The VLa decrease reached significance 50 ms after GPi pause onset. Given that GPi pauses had a mean duration of 195 ms, the decrease in VLa firing rate occurred during GPi pauses, not following them. Population averaged cross-correlations of the times of pauses in GPi unit activity relative to burst offsets for the same unit (Fig. 5 D) showed a broad (>200 ms) period of negative correlation (i.e., reduced likelihood of a pause) at negative time lags, as would be expected because pauses in firing are unlikely to occur during bursts. The probability of a pause swung sharply to positive values at the time of burst offset and remained positive for >500 ms thereafter. Thus, bursts and pauses in GPi activity tended to occur together in that order, with decreases in VLa firing rates occurring following GPi bursts, during GPi pauses.

An analysis of individual GPi-VLa cell pairs provided results consistent with the population-level burst/pause analysis. Only small fractions of GPi-VLa pairs showed any significant change in VLa activity following GPi burst onsets, burst offsets, or pause onsets (*Burst/pause influences*; Table 2). Among those significant effects, decreases in VLa firing rate were far more common than increases, composing more than two-thirds of the significant effects for all events (*Burst/pause influences*; Table 2). Due to the small number of cases, however, those differences in prevalence were only nominally significant and only so for burst onset and offset (p=0.04, 0.05 and 0.16 for burst onset, burst offset and pause onset, respectively; chi-square test).

Together, these results suggest that the activity of some GPi-VLa neuron pairs is coordinated such that burst-pause complexes in the GPi neuron's activity are associated with long-lasting reductions in the firing rate of the VLa neuron. The characteristics of this phenomenon, however, are not consistent with predictions of either gating or rebound models.

Insert Figure 5 around here

VLa activity relative to GPi bursts and pauses. A-C: Population average VLa firing rates relative to GPi burst onsets (A), burst offsets (B), and pause onsets (C). The 95% confidence interval is shown in gray. In all three cases, VLa firing rates drop and stay low for several hundred milliseconds. D: Population average cross-correlation of GPi pause onset times relative to the times of GPi burst offset (mean +/- SEM). Pauses in GPi activity were more likely to occur immediately following the offset of a GPi burst.

Data and code to reproduce this figure can be found in https://doi.org/10.5061/dryad.0cfxpnvxm (Fig5_S14.m).

Simulations suggest GPi-VLa communication scales with GPi synchrony and convergence

Given that GPi neurons project to VLa, it would be surprising if this pathway did not serve a functional role. Because we observed little impact of GPi activity on VLa in our empirical data, we turned to computational simulations to explore possible relationships between spiking in GPi and VLa (Fig. 6). Specifically, we computationally generated sets of N GPi spike trains, with pairwise correlations c, for various choices of N and c. These N spike trains provided converging inhibitory inputs to a single model thalamocortical relay cell in which synaptic conductances were normalized by 1/N to maintain a constant average synaptic conductance across different choices of N (Fig. 6A). (Homeostatic normalization of synaptic inputs similar to this is common in thalamocortical neurons [55].) Cross-correlations between spike times from randomly selected GPi input trains and the VLa neuron were computed for lags in the interval [-100 ms, 100 ms], and averages from 20 GPi neurons were collected over 4 separate runs for each (N,c) pair. Results showed a clear growth of the post-spike inhibition of VLa with increasing c (GPi pairwise correlation) when the number of converging GPi neurons (N) is held constant (Fig. 6 B). Importantly, when the within-GPi correlation is held constant, the post-spike inhibition of VLa decreased in magnitude as the number of converging GPi neurons (N) increased. Average correlations in the interval [0ms,10ms] were approximately proportional to c(N-1)/N+1/N as

predicted on theoretical grounds (Fig. 6C; see also *Materials and methods*). For large N and small c, the relative influence of individual GPi spike trains on VLa spiking became small due to a large number of GPi spike trains contributing uncorrelated variability to the VLa membrane potential. Given a certain fixed amount of inhibition to each VLa neuron, these results highlight the importance of the degree of anatomical convergence from BG output neurons onto recipient thalamic neurons, which is reported to differ markedly between homologous circuits in the songbird (in which N=1; [25; 35]) and mammals (in which N may exceed 20). They also suggest that in contexts in which pairwise GPi cross-correlations are elevated (e.g., in parkinsonism [56; 57]), GPi outputs may exert a strong influence on subsequent VLa activity. Significant pairwise correlations in GPi spiking are rare, however, under baseline behavioral conditions in neurologically-normal animals [56; 58; 59]. We confirmed that observation in the current dataset by finding only 13 significant spike-to-spike correlations among 148 pairs of GPi neurons examined (Supporting Information S12 A). Out of these 13 significant correlations, three were classified as strong outliers (>10×median absolute deviation away from the population median). While the mean of all CCFs just exceeded the threshold for significance (Supporting Information S12 D, *black* line), that significance was lost after removal of those three outliers (Supporting Information S12 D, *dashed* line). No strong outliers were observed for the rest and movement periods (Supporting Information S12 B-C) or for any GPi-VLa correlation (Fig. 4).

In summary, the simulation results suggest that our empirical data were collected under conditions approximated by the model with parameters in the range of N≥20 and c<0.1 (i.e., high GPi-to-VLa convergence and low intra-GPi synchrony). Changes of those conditions, for example increases in synchrony within GPi, may lead to efficient inhibition of thalamus by BG output.

Insert Figure 6 around here

GPi synchrony and anatomical convergence determine correlations between GPi and VLa. A: Computational model architecture. One VLa neuron is inhibited by N GPi neurons with pairwise correlation c. B: Population average cross-correlations across (N,c) combinations. C: Average correlations in the interval [0ms,10ms] are similar to a linear approximation (dashed lines; see Materials and methods for details). Bars indicate the standard error of the mean of the 20 trials.

Data and code to reproduce this figure can be found in https://doi.org/10.5061/dryad.0cfxpnvxm (Fig6.m).

Discussion

It is often assumed that task-related changes in neuronal activity in BG-recipient regions of thalamus are permitted or caused by the temporal pattern of input from the BG. The physiologic mechanisms most often cited are some kind of gated permission to spike [12; 14; 15] or a triggering of rebound spikes in thalamus through release from sustained inhibition [20; 21; 22]. Recently, Goldberg and Fee [25] demonstrated in the awake songbird that thalamic neuron spiking can be entrained to the inter-spike intervals of ongoing pallidal spiking, not only during overt pauses in pallidal firing as proposed by the standard gating model. None of these models have been tested before in the NHP. Here, we sampled single-unit activity simultaneously from connected regions of GPi and VLa thalamus during performance of a reaching task. We searched for evidence consistent with a gating or rebound sculpting of thalamic activity by BG output. Some of our results also bear on the entrainment model. The contrast between our observations against the main predictions of the gating and rebound theories is summarized in Table 3.

We found that peri-movement modulations in discharge were very common in GPi and VLa. Critically, those modulations consisted of increases in discharge more often than decreases both in GPi and in VLa. This finding was supported by two independent analyses: first of the signs

(increase vs. decrease) of individual response profiles, and second of integrated changes in firing across the movement period. It is difficult to reconcile these results with the gating hypothesis without invoking some yet undiscovered mechanism that would make decrease-type responses in GPi, which were in the minority in our observations, more effective at eliciting VLa spikes than increase-type responses are at inhibiting them (e.g., Goldberg et al.'s [2] "different motor channels" idea).

Both gating and rebound hypotheses predict that task-related changes in GPi activity should begin earlier in time than the neuronal responses they are hypothesized to elicit in thalamus. Contrary to those predictions, we found that onset latencies of GPi responses lagged in time behind those of VLa responses. That was true for a comparison of all responses and, most directly relevant to the hypotheses, for comparisons of GPi decreases versus VLa increases and GPi increases versus VLa decreases. Together, these results bring into question the idea that task-related activity in VLa is generated or permitted by changes in GPi activity. Instead, they buttress previous suggestions [24; 25] that task-related activity in BG-recipient regions of thalamus is generated primarily by some non-BG source (e.g., by glutamatergic inputs from cortex [60; 61]) and that uncorrelated BG inputs have a more subtle influence on thalamic activity than often assumed.

The qualitative form of peri-movement modulations in discharge as well as their timing were comparable between movement directions. Restricting analyzes to the preferred direction of each neuron did not change our main findings, stressing the absence of evidence for direction-selective gating or rebound. Compared to rodents [42], the general direction-selectivity of neurons in the basal ganglia recorded here was rather weak. That discrepancy may relate to differences in the tasks used for rodents

and our NHPs: rodent tasks often [42; 62] (but not always [44; 63]) require large movements of the body in opposing (e.g., left vs. right) directions. In contrast, our NHPs performed discrete reaches with one arm toward one of two targets that were positioned only 14 cm apart such that muscle activity for those two reach directions differed only quantitatively (Supplementary Information S3). We cannot rule out the possibility that a task that required selection between categorically different movements would have yielded results more consistent with gating or rebound hypotheses. It is worth noting, however, that our latency results, in which GPi responses began largely after the onset of agonist EMG, agree with many previous studies that used a wide variety of motor tasks performed in NHPs [31; 32; 28; 64] and in rodents [65].

Another approach to test for possible influences of GPi input on VLa activity is to determine the pattern of correlated activity observed in simultaneously-recorded GPi-VLa cell pairs. This approach has the potential to elucidate the nature of cell-to-cell communication and how it differs between task conditions [66]. (See below for caveats concerning this approach.) It is revealing that very few GPi-VLa cell pairs (<6%) showed significant spike-to-spike correlations, and in those few, the correlations were small in magnitude (peak variation in firing rate < 30% of the baseline rate) and independent of task period (i.e., during rest or movement periods). Moreover, the whole population of cross-correlations was similar to a control distribution with jittered spike times. We used simulated Poisson spike trains with known underlying correlations to rate the sensitivity of our method, and excluded pairs with sparse data that did not allow for detection of small correlations. The result differs markedly from the common assumption, as predicted by gating and rebound hypotheses, that cross-correlations for connected GPi-VLa cell pairs will be strongly negative. It also differs from the strong negative cross-correlations observed by Goldberg and Fee in the songbird BG-thalamic circuit [25]. Our simulations

illustrate how the absence of strong cross-correlations in our data may be accounted for by the anatomical convergence, in mammals, of inputs from numerous GPi neurons onto individual VLa neurons [10; 36] as compared with the 1:1 pairing in the songbird of very strong calyceal-type synaptic contacts from single pallidal axons onto an individual thalamic neuron [35].

Proper evaluation of the correlation results discussed above requires consideration of how likely it was for our recordings to encounter synaptically-connected GPi-VLa cell pairs. Even though recordings were restricted to regions of the GPi and VLa that were likely to be connected (i.e., regions responsive to stimulation of arm M1), single-units were sampled at random from within those regions. The likelihood of recording from connected pairs depends on the detailed anatomy of GPi projections into VLa. Axons of individual GPi neurons terminate in multiple dense glomerule-like clusters in the VLa, up to 10 of which are distributed widely across the VLa [11; 36; 67]. Within each cluster, large multi-synapse boutons contact primarily the somata and proximal dendrites of multiple thalamocortical projection neurons [10; 11; 36]. Thus, although exact quantification of the degree of GPi-to-VLa divergence has yet to be performed, it is clear that individual GPi neurons diverge to contact numerous thalamic neurons distributed across the VLa. This anatomic arrangement should markedly improve our chances of encountering connected GPi-VLa pairs by random sampling. The paucity of evidence for connected GPi-VLa cell pairs in our cross-correlation results implies either that the degree of GPi-to-VLa divergence is more sparse than what the anatomy suggests or that the influence of individual GPi cell firing on the recipient VLa neuron was far more subtle in our paradigm than what current theories would predict.

An influence of GPi inputs on VLa activity might also be evident in slow trial-to-trial covariations in the firing rates observed within GPi-VLa cell pairs (noise correlations). If a

gating mechanism dominated GPi-VLa communication, then the majority of significant noise correlations would be expected to be negative and/or the overall distribution might be biased toward negative correlations. Noise correlations in our data were occasionally significant (5% of pairs at rest and 7% of pairs during movement), but these were composed of balanced proportions of positive and negative correlations (Fig. 4G-H) and the overall distribution of noise correlations did not differ from a shuffled control. Significant noise correlations can be produced by a variety of mechanisms other than direct monosynaptic connectivity, which include, most obviously, co-modulation of both neurons in the pair by a third source of input [68].

Bursts and pauses in GPi activity are prolonged neurophysiologic events likely to have more profound effects on post-synaptic neurons than the effects of single spikes [54; 69]. Most important here, a burst of inhibitory GPi input to a thalamic neuron followed by a pause in firing should be an ideal stimulus to trigger rebound-type spiking – if, that is, the rebound mechanism is in effect. As others have described previously [54], we found that spontaneous bursts in GPi firing during periods of attentive rest are often followed by pauses. However, these burst-pause events in GPi neurons were coupled with small yet sustained *reductions* in mean VLa firing rate, thus opposite of what the rebound mechanism predicts. Critically, those reductions in firing rate occurred at around 119ms after burst onset and were thus much slower than what would be expected for the synaptic transmission (compare to Fig. 1 B: VLa was inhibited few milliseconds after GPi stimulation). The lack of VLa rebound responses following GPi pauses in our trials involving successful movements dovetails with the lack of motor impairments found in Cav3.1 knockout mice that lacked thalamic rebound firing [22]. Moreover, both the timing and sign of the observed VLa rate changes were inconsistent with predictions of the gating hypothesis. The observed co-occurrence of VLa firing rate reductions with GPi burst-pause complexes may

reflect large-scale properties of the BG-thalamo-cortical network, similar to those invoked previously to explain the detailed structure of bursts and pauses in pallidal activity [54; 70]. Regardless of that, our results are not consistent with straightforward interpretations of gating or rebound models, both of which hypothesize that thalamic activity is strongly determined by BG output.

While our results are restricted to a well-learned movement task and rest, which both involve low synchrony of BG output [56; 59](Supporting Information S12), effective thalamic inhibition or excitation may be possible in the presence of BG synchrony. To demonstrate this reasoning, we simulated a simplified version of the recorded circuit (Fig. 6). Our simulations confirm that in the presence of anatomical convergence from BG to thalamus and low synchrony of BG output, thalamus is only weakly affected by the BG. In contrast, synchrony of BG output can lead to efficient short-latency inhibition of thalamus, even in the presence of strong convergence. We therefore suggest that BG output correlations can be a powerful modulator of basal ganglia influences on thalamus, which may be exploited under specific behavior conditions (e.g., during reward-based learning) and may be a factor in the pathophysiology of BG disorders [56; 57].

To our knowledge, this is the first study of single-unit activity sampled simultaneously from the GPi and VLa. These results, though novel, are consistent with many previous observations. Past between-studies comparisons observed that task-related increases in firing are more prevalent than decreases both in BG-output neurons [28; 29; 30; 31; 32] and in VLa thalamus [33] (69%); [17] (83%); [34]. The latencies of task-related activity in BG output neurons [28; 31; 32] also appeared to lag in time behind those in VLa [17; 33; 34]. Our results are consistent with several past reports that movement-related modulations in GPi activity begin after the onset of activity in the agonist muscles but before the onset of overt movement [28; 30; 31].

In addition, task-related changes in VLa activity were unaffected by temporary inactivations of the GPi [24], even though the background firing rate of VLa neurons increased during those inactivations. More recently, Goldberg and Fee [25] confirmed in the songbird BG-thalamic circuit the paradoxical presence of task-related increases in activity both in BG output neurons and in BG-recipient thalamus and the persistence of task-related activity in the BG-recipient thalamus following ablation of the BG. The present results are also consistent with the more general observation that inactivations or ablations placed in BG output nuclei have, at most, minor detrimental effects on the performance of familiar motor tasks both in human patients [71; 72; 73; 74] and in neurologically-normal non-human animals [24; 75; 76; 77; 78].

Given the lack of strong gating or rebound, how can we explain co-activation of GPi and VLa with movement? Rodent layer 5 pyramidal tract neurons of motor cortical areas innervate both BG and BG-recipient thalamus [79; 80]. Thus, excitatory drive from motor cortex at with different delays may explain our observation of strong movement-related modulations in firing rate in both GPi and VLa without evidence for strong direct interactions between the two nuclei. Indeed, electrophysiological evidence indicates an efficient excitatory cortical control of motor thalamus [63; 81], possibly explaining the early activation of VLa with movement onset.

Finally, how do we bring the current results into coherence with other studies that demonstrated strong BG-thalamic effects? For example, two recent studies showed that optogenetic stimulation of BG output had profound effects on thalamic activity [22; 82]. Stimulation produced thalamic firing rate changes along with differences in licking behavior [82], and was followed (at a lag of ~70 ms) by a sharp rebound-like increase in thalamic spiking accompanied by muscle contractions [22]. Based on the timing reported there, any similar post-inhibitory rebound in our data would have been apparent in our GPi burst-pause analysis (Fig. 5), yet we

saw a decrease rather than an increase in thalamic firing. As shown by our model (Fig. 6), the impact of convergent BG inputs to a recipient thalamic neurons depends tremendously on the degree of synchronization in spiking between those BG inputs. Obviously, massed stimulation of BG efferent terminals (e.g., using optogenetic methods as in [22; 82]) will induce a synchronized volley of action potentials in a large fraction of the BG output neurons. Similarly, macroelectrode stimulation of GPi, which inhibited VLa activity in our animals (Fig. 1B), induces a volley of action potentials synchronized across a large population of GPi neurons [83]. Also rodent work has revealed a potent effect of synchronized compared to uncorrelated SNr activity [84]. Our simulation (Fig. 6) shows how such a synchronized population volley (i.e., high level of pairwise correlation c) will have a much larger post-synaptic influence on thalamic neurons than that of the highly de-synchronized spiking that is typical of a non-perturbed population of BG output neurons [56; 58; 59] (see also Supporting Information S12). Note that our observation of very low levels of between-neuron synchrony in GPi is consistent with multiple past studies in neurologically-normal animals [59; 85], even during performance of well-learned behavioral tasks [56; 86]. The primary BG output nucleus in the rodent (SNr) shows similarly low levels of pairwise correlations [87], potentially due to desynchronization by intrinsic inhibitory connections [88].

Potential limitations and caveats

As discussed above, our results describe the dynamics of randomly sampled pairs of neurons in GPi and VLa and they do not rule out the possibility that strong interactions, including gating or rebound, exist within tightly focused sub-circuits connecting those nuclei. For example, it would be nearly impossible to detect by random sampling the very strong

entrainment-like interactions observed in the hyper-focused pallido-thalamic circuit of the songbird [25; 35]. The anatomy of the mammalian GPi-VLa projection, however, suggests a far more branched organization containing a great deal of divergence and convergence [10; 11] in which it should be possible to study connected cell pairs by random sampling from GPi and VLa. At minimum, our results put a low upper limit (i.e., less than 15 in 427, see Table 2) on the probability of finding strong spike-to-spike cross-correlation effects, if any exist, in randomly selected GPi-VLa cell pairs. In addition, our results are inconsistent with the classic gating idea in which a coordinated drop in GPi activity is required to release thalamic activity and subsequent selection of action [40; 41].

In the comparison of onset latencies for GPi and VLa responses, a substantial degree of overlap in the distributions (Fig. 3 and Supporting Information S8) leaves open the possibility for gating-like latency relationships in a minor subpopulation of GPi and VLa neurons. However, gating-consistent relationships of response sign and timing were found in only a small fraction (4%) of all possible combinations of GPi and VLa responses. In addition, inconsistent results for GPi and VLa were found when we tested for relations between response latencies and response magnitudes. Early latency responses in VLa were larger in magnitude than later responses whereas GPi responses did not vary in magnitude as a function of latency (Supporting Information S9). Furthermore, our study of cross-correlations and noise correlations in simultaneously recorded GPi-VLa pairs did not reveal any indication of gating or rebound mechanisms (Fig. 4).

It is also important to acknowledge that we studied GPi-VLa communication during performance of a simple well-learned reaching task. It is possible that the influences of BG output on thalamic spiking could be stronger under more demanding or less-stereotyped behavioral contexts. For

example, several lines of evidence suggest that BG-thalamic pathways drive behavioral variability or exploration during motor learning [89; 90; 91]. Other studies suggest BG involvement in the on-line modulation of movement vigor [44; 75] or the urgency to move [45]. A growing number of studies have concluded that the influence of BG output on a behavior becomes less important the more well-learned the behavior becomes [27; 77; 92]. It is possible that, under one or more of those less-stereotyped behavioral contexts, task-related activity in the GPi may adopt characteristics more capable of influencing VLa activity (e.g., larger firing rates, shorter latency responses to inputs, or more synchronization of spiking between GPi single-units).

Conclusion

In conclusion, we found no evidence consistent with the idea that BG output discharge gates thalamic discharge ('classic gating hypothesis', [12]). The most likely alternative is that both pallidal and thalamic discharge may be driven by a third source [24; 25]. Layer 5 projections from motor cortex are a reasonable candidate for shared excitatory drive [63; 80; 81]. To the extent that they have been compared, all BG-thalamic projections in mammals appear to share similar anatomy and physiology [10]. Because of that, the present results have important implications for BG-thalamic communication in all functional circuits (e.g., in associative, oculomotor and limbic functional circuits [38]), not just the skeletomotor circuit. Our results are compatible with the idea that BG outputs may counter-balance cortical drive to thalamus. For example, increases in BG output may modulate or constrain the magnitude of thalamic changes in discharge, perhaps as a consequence of recent reward history [2]. Finally, subtle changes in BG output synchrony may be a potent way to scale the effectiveness of inhibitory drive to thalamus.

Materials and methods

Data collection

Animals and Task

Two monkeys (Macaca mulatta; G, female 7.1kg; I, female 7.5kg) were used in this study at the University of Pittsburgh. All aspects of animal care were in accord with the National Institutes of Health Guide for the Care and Use of Laboratory Animals, the PHS Policy on the Humane Care and Use of Laboratory Animals, and the American Physiological Society's Guiding Principles in the Care and Use of Animals. We made all efforts to provide excellent animal care and to alleviate unnecessary discomfort. All surgical procedures were carried out under general anesthesia, using sterile techniques in approved surgery areas. Analgesics were used postoperatively to minimize discomfort or pain. All experimental protocols were performed in strict accordance with the National Institutes of Health Guide for the Care and Use of Laboratory Animals and were reviewed and approved by the University of Pittsburgh IACUC before the studies began (ACUC protocol number 18093682). The animals performed a choice reaction time reaching task that has been described in detail previously [48; 49]. In brief, the animal faced a vertical response panel that contained two target LEDs, positioned 7 cm to the left and right of midline, and associated infrared proximity sensors. The animal's left hand rested at a "home-position" at waist height and equipped with a proximity sensor. The animal was trained to hold the home-position (1–2s, uniform random distribution) until the right or left LED was lit as a directional "Go" signal (selected in pseudo-random order). The animal was given 1s to move its hand from the home-position to the indicated target. Once the correct target was contacted, the

animal was required to hold its hand at the target for 0.5–1.0s (randomized) before food reward was delivered via a sipper tube and computer-controlled peristaltic pump. The animal was then allowed to return its hand to the home-position with no time limit. The right hand was restrained in a padded splint at the animal's right side.

Surgery

General surgical procedures have been described previously [49; 75]. The chamber implantation surgery was performed under sterile conditions with ketamine induction followed by isoflurane anesthesia. Vital signs (i.e. pulse rate, blood pressure, respiration, end-tidal pCO_2, and EKG) were monitored continuously to ensure proper anesthesia. A cylindrical titanium recording chamber was affixed to the skull at stereotaxic coordinates to allow access to the right globus pallidus and ventrolateral thalamus via a parasagittal approach. A second chamber was positioned over the right hemisphere in the coronal plane to allow chronic implantation of stimulating electrodes in the arm area of primary motor cortex and the decussation of the superior cerebellar peduncle (SCP). The chambers and head stabilization devices were fastened to the skull via bone screws and methyl methacrylate polymer. Prophylactic antibiotics and analgesics were administered post-surgically.

A second aseptic surgery was performed in one animal (NHP G), to implant chronic subcutaneous electrodes for electromyographic recording [75]. Pairs of fine Teflon-insulated Stainless steel wires (AS632 Cooner Wire) were implanted into six muscles of the proximal arm (biceps, triceps, anterior and posterior deltoid, pectoralis and latissimus dorsi). The wires were tunneled subcutaneously to a connector mounted on the animal's cranial implant.

Localization of stimulation sites and implantation of indwelling macroelectrodes

To guide an electrical stimulation-based localization of the region of GPi devoted to arm motor control [93] and of the connected region of VLa [34] we implanted stimulation electrodes in the arm-related region of primary motor cortex and in the SCP at its decussation (Fig. 1). The anatomic locations of sites for implantation were estimated initially from structural MRI scans (Siemens 3T Allegra Scanner, voxel size of 0.6mm) using an interactive 3D software system (Cicerone) to visualize MRI images and predict trajectories for microelectrode penetrations [94]. Subsequent microelectrode mapping methods were used to identify the precise chamber coordinates for the implantation.

Custom-built stimulating electrodes were implanted at these sites using methods described previously [95]. Macroelectrodes consisted of two Teflon-insulated Pt-Ir microwires (50µm) glued inside a short stainless-steel cannula with ~0.5mm separation between the distal ends of the microwires. Insulation was stripped from ~0.2mm of the distal ends of the microwire to achieve an impedance of ~10kΩ. The electrode assembly was implanted transdurally via the coronal chamber using a protective guide cannula and stylus mounted in the microdrive. In the months following implantation, the location and integrity of macroelectrodes were monitored by comparing the muscle contractions evoked by stimulation through the electrode against what was observed during microelectrode mapping.

Localization of target regions for recording in GPi and VLa

The chamber coordinates for candidate regions in GPi and VLa were estimated initially from structural MRIs as described above. Target region localization was then refined using single unit

microelectrode recording in combination with electrical stimulation through electrodes in SCP and GPi (single biphasic pulses <200μA, 0.2ms-duration at 2Hz max.; Model 2100, A-M Systems; Fig. 1) and proprioceptive stimulation. The target region for recording in GPi was identified by the presence of typical high firing rate single-units, many of which responded briskly to proprioceptive stimulation of the forelimb [32; 96] and responses to electrical stimulation in the arm region of primary motor cortex [93] (Fig. 1C). During localization of the target region in VLa, a macroelectrode was positioned acutely in the GPi. The target region for recording in VLa was identified by the presence of typical thalamic neuronal discharge that: a) responded to GPi stimulation with a short latency pause in firing [34] often followed by a rebound increase in firing probability; and b) did *not* respond to SCP stimulation, which would be indicative of a neuron in VLp, the cerebellar-recipient portion of motor thalamus located immediately posterior to VLa (Fig. 1B). Many VLa neurons also responded at short latency to stimulation in primary motor cortex. All subsequent data collection was directed to these target regions of GPi and VLa.

We also performed microstimulation mapping of VLa and VLp (biphasic pulses <200μA, 0.2ms-duration at 300Hz; Model 2100, A-M Systems). Consistent with previous reports, stimulation in putative VLa rarely evoked movement whereas stimulation in putative VLp evoked movement often and at low threshold [97; 98]. However, it was possible to evoke movement from some locations close to VLp but identified as VLa according to the localization criteria described above. Thus, results from microstimulation mapping of the thalamus were not used as primary criteria for identification of the VLa/VLp border.

Recording protocol

The extracellular spiking activity of neurons in GPi and VLa was recorded using multiple glass-insulated tungsten microelectrodes (0.5–1.5MΩ, Alpha Omega Co.) or 16-contact linear probes (0.5–1.0MΩ, V-probe, Plexon Inc.). Data were amplified (4×, 2Hz–7.5kHz), digitized at 24 kHz (16-bit resolution; Tucker Davis Technologies), and saved to disk as continuous data.

All recordings were performed with at least one electrode positioned in each of GPi and VLa. When stable single-unit isolation was available from one or more single-units in both GPi and VLa, as judged by online spike sorting, neuronal data and behavioral event codes were collected while the animal performed the behavioral task.

During a subset of data collection sessions EMG activity was collected via either chronically-implanted subcutaneous electrodes (NHP G) or electrodes inserted percutaneously immediately before the session (NHP I). The EMG signals were amplified (4×), band-pass filtered (100–5000Hz), digitized (6104 Hz), rectified, low-pass filtered (500 Hz) and then down-sampled to 1017 Hz.

Offline analysis

Behavior

Task performance was screened to exclude error trials and outliers in task performance. Reaction times reflected the time interval between LED lighting and subsequent offset of the home position proximity detector. Movement durations reflected the time interval between detected departure from the home position and detected arrival of the hand at the target. Outliers in

reaction time or movement duration were defined as values >6×median absolute difference away from the mean (Matlab TRIM).

Spike sorting and detection of peri-movement discharge

The stored neuronal data were high-pass filtered (Fpass: 300Hz, Matlab FIRPM) and thresholded, and candidate action potentials were sorted into clusters in principal components space (Off-line Sorter, Plexon Inc.). Clusters were accepted as well-isolated single-units only if the unit's action potentials were of a consistent shape and could be separated reliably from the waveforms of other neurons as well as from background noise throughout the period of recording. Times of spike occurrence were saved at millisecond accuracy.

Single-units were accepted for further analysis if they met the following *a priori* criteria. A minimum of 10 valid behavioral trials was required for all task-based analyses. [Among the single units studied the actual minimum number of trials collected (16) was greater than this *a priori* minimum.] The minimum firing rate, mean across the whole period of recording, was 30 Hz for GPi units and 1 Hz for VLa units.

We tested for peri-movement changes in single-unit spike rate using a standard method [49] that was modified to improve the sensitivity to firing rate decreases through use of different estimates of unit activity for the detection of increases and decreases in discharge. For increases, we used a standard spike density function (SDF), which correlates directly with a neuron's mean instantaneous firing rate. For decreases, however, we used a function that reflects a unit's instantaneous inter-spike interval (ISI) [99] which scales with the reciprocal of a neuron's instantaneous spike rate. Use of the ISI function avoided a potential insensitivity for the

detection of decreases in SDFs due to floor effects, which would be particularly problematic for low firing-rate neurons such as those in VLa. (By definition, the minimum value for an SDF is zero spikes/s regardless of the duration of a pause in firing, whereas an ISI function can reliably represent arbitrarily long pauses in firing.) SDFs were constructed by convolving a unit's spike time stamps (1 kHz resolution) with a Gaussian kernel (σ = 25 ms). ISI functions were calculated as a millisecond-by-millisecond representation of the current time interval between successive single-unit spikes smoothed (Matlab CONV) using a 25ms Gaussian kernel. Across-trial mean SDF and ISI functions aligned on the time of movement onset were constructed separately for valid behavioral trials to left and right targets.

The detection algorithm then tested both SDF and ISI activity functions for significant positive deviations from a control rate within a 700 ms window that started at the median time of target LED onset relative to the time of movement onset (i.e., within a time period that encompassed both reaction time and movement duration for our animals). The threshold for significance was defined relative to the mean and SD of values from a pre-trigger control period (a 700 ms window that ended at the median time of target LED onset) after any linear trend in the mean activity function from that period was subtracted. A movement-related change in firing rate was defined as a significant elevation from the control mean activity that lasted at least 70 ms (e.g., Fig. 2 A, *solid vertical lines*; *t-test*; point-by-point comparisons at 1 ms resolution of one sample vs. control period mean; omnibus $p < 0.001$ after Bonferroni correction for multiple comparisons). Any such elevations in the SDF were classified as increases in discharge whereas elevations in the ISI function were classified as decreases in discharge. Note that this approach enabled detection of biphasic changes (e.g., an increase followed by a decrease).

To test for potential biases in the response detection algorithm, we generated simulated data with imposed responses of different sizes and then measured the sensitivity of our algorithm to detection of those simulated responses. For each single-unit in our empirical database, we generated simulated SDF and ISI activity functions (for detection of increases and decreases, respectively) based on that unit's pre-trigger control period mean (μ) and SD (σ). Each simulated activity function was 1500 ms long. For each 25 ms interval of the first 1000 ms, values were chosen from a normal distribution matching the experimental μ and σ. For the period 1000–1500 ms, a simulated response was imposed by selecting values from a normal distribution with mean $\alpha\mu$ and SD σ, where α reflects the change in activity expressed as a fraction of baseline. These values were then interpolated using Matlab's cubic spline interpolator resulting in a simulated activity function that matched both the statistics and the qualitative features of the empirical data. One hundred such SDF and ISI activity functions were created for each single-unit and level of α (at intervals of 0.05 between $\alpha = 0.0$ and 3.0). The detection algorithm was applied to all simulated activity functions and the fraction of responses detected was quantified as a function of α, single-unit type (GPi vs. VLa) and response sign (increases vs. decrease). See Supporting Information S5 and associated caption for a summary of the results from this simulation.

For each significant movement-related change detected, we used two independent approaches to estimate the time of onset (i.e., the latency). The first standard approach [49; 95] simply took the earliest significant time bin yielded by the detection algorithm described above. To ensure that the standard approach did not provide biased results, we also applied a second approach which defined onset as the time at which the mean activity function crossed a threshold corresponding to 10% of the maximum change in rate relative to the control rate (as defined above).

The accuracy of the latency estimation algorithm was tested by applying it to simulated responses that had known onset latencies but otherwise matched the statistics of empirically-observed responses. For each increase-type response detected, we created a simulated increase-type response by imposing onto that unit's baseline (±SD) firing rate a trapezoidal increase in firing rate that matched the magnitude and onset slope of the empirical response. Likewise, for each decrease-type response detected, we created matching simulated ISI changes from the baseline ISI (±SD). The latency estimation algorithm described above was then applied to these simulated increase- and decrease-type responses. This analysis revealed a slight non-significant bias in the algorithm toward detecting GPi responses earlier than VLa responses (Supporting Information S7). Note that this bias is the converse of the actual difference in latencies observed between GPi and VLa.

To investigate the possibility that response latency results differed depending on a unit's preferred direction, we tested for significant differences in response magnitude as a function of movement direction and then identified the neuron's preferred direction. First, we tested for significant differences in a neuron's firing rate for movements to left and right targets. Trial-by-trial spike counts from a 300 ms window starting at the unit's earliest detected response onset were compared between left- and right-target trials. If a unit's spike rate differed significantly between the two movement directions ($p<0.005$; Matlab RANKSUM), then the unit's "preferred direction" was defined as the direction for which spike rate during the same 300 ms window differed (i.e., either increased or decreased) the most from baseline firing rate.

Spike and rate correlations

To estimate the level of fast coordination between spike times in GPi and VLa, we computed cross-correlation functions (CCFs). Spike time series were kept uncut ('whole recordings') or cut trial-by-trial into 0.5 s-long windows aligned to the time of movement (-0.2 to 0.3 s relative to detected movement onset) or to the pre-go cue rest period (1.5 to 1 s before detected movement onset). GPi units with average firing rates below 30 Hz, VLa units with firing rates below 1 Hz, as well as all units with a total spike count of less than 100 within all relevant trials were excluded. For all other pairs recorded simultaneously in GPi and VLa, the normalized CCF

$$CCF(\tau) = \frac{\sum_{s=1}^{n} y(t_s + \tau)}{n\,\overline{y(t)}}$$

was computed for time lags $\tau \leq 200ms$, taking advantage of zero-padding, and averaged over all trials of a recording. t_s denotes the s=1,…n spike times of the GPi neuron, *y(t)* the binary spike time series of the VLa neuron, and $\overline{y(t)}$ the average VLa firing rate. Surrogate time series were generated by randomly jittering spike times within intervals of 20 ms as suggested by Amarasingham et al. [100]. This kind of surrogate data left local firing rates unchanged while removing spike synchrony on a timescale of 20 ms or shorter and thereby serving as a negative control for spike synchrony. Average CCFs of surrogate data were subtracted from both trial averaged CCFs for each GPi-VLa unit pair as well as from all control CCFs. All final CCFs were rated by the absolute value of the maximum deviation from zero in the time interval [0,10]ms ([-5,5]ms for CCFs between GPi neurons) after smoothing with a 2ms moving average filter. Additionally, to control for false negative findings, we simulated Poisson spike trains with known correlations. For each recorded pair, 400 simulated spike trains were matched to the firing rates of GPi and VLa neurons and to peak correlations of value *p* for very long recording times.

By subsampling those simulated spike trains at the length of our recordings, we observed simulated distributions of correlations around the underlying correlation p. This procedure allowed us to determine the minimum reliably detectable correlation c_0 for each pair. c_0 was defined as the lowest p for which 95% of the distribution of simulated correlations was larger than 95% of the control distribution. Thus, c_0 can be used to rate the sensitivity of correlation detection in each pair. If $c_0 > 0.3$, the pair was excluded from the analysis. Moreover, the approach allowed for estimation of upper bounds c_u of the measured correlations. c_u was defined as the lowest p for which 95% of the simulated correlations were larger than the measured correlation. c_u therefore sets an upper limit to the correlations in our system.

Next, we tested whether correlations in trial-by-trial variations in firing rates ('noise correlations') between GPi and VLa discharge were present. We computed spike counts in 500 ms bins within the same rest and movement periods as used for CCFs. If the total spike count in a time bin across all trials of a unit was lower than 10, the bin of this unit was excluded. Spike counts were z-scored and trials with a score > 3 were removed from further analysis, as described by Liu et al. [101]. Separately for each pair and each of the two targets, correlations were then computed across bins of spike counts. Simultaneous modulations of firing rates that occur consistently across movements are thus not reflected in the noise correlations. Instead, only trial-by-trial variations of rate contribute. Randomly shuffling trials within each recording served as surrogate data.

Analysis of bursts and pauses

The classic gating hypothesis states that any increased BG output, regardless of its relation to movement timing, can attenuate thalamic spiking [13]. Here, we investigated the influence of

GPi bursts and pauses on VLa spiking during rest. Bursts were detected with a 'surprise' method developed by Legéndy & Salcman [102] and implemented by Wichmann & Soares [54]. The surprise value was defined as S=-log(P), where P is the probability that the distribution of inter-spike-intervals within the candidate burst is from a Poisson distribution. Only bursts with a surprise value of 5 or larger, with at least three spikes and an intra-burst firing rate of at least twice the baseline firing rate, were considered. Likewise, pauses were defined as inter-spike-intervals of at least 100ms with a minimum surprise value of 5. All bursts and pauses that were detected during the time period when the task was performed (from 0.4 s before detected movement onset until 0.8 s after return to the home key) were excluded. As movement periods were associated with strong modulations in firing rate (see Fig. 2), reliable burst and pause detection during these periods was not possible.

VLa spike trains were convolved with a Gaussian density of standard deviation $\sigma = 10$ ms. We then averaged all epochs of VLa spiking from 0.8 s before to 0.8 s after GPi burst onset and called this average spike train a burst-triggered average (BTA). Each simultaneously recorded GPi-VLa pair thus led to one BTA. We used the same analysis with alignment to burst end to determine burst-offset-triggered averages (BOTAs) and with alignment to pause onsets for pause-triggered averages (PTAs). Some pairs included few GPi bursts or low baseline firing rates in VLa, impeding the detection of burst or pause influences. To avoid including such noisy data, we excluded GPi-VLa pairs with noisy pre-burst baselines, defined as the average VLa activity 800 – 50 ms prior to the respective event (GPi burst onset, offset, or pause): If the difference between the 2.5^{th} and the 97.5^{th} percentile of this baseline was larger than 60% of the absolute average baseline activity, the respective GPi-VLa pair was neglected. Hence, only pairs with a rather constant, predictable baseline were included in the analysis.

All obtained TAs of each type (BTAs, BOTAs, and PTAs) were averaged to compute a population average TA of that type. We also evaluated whether some VLa units showed a significantly high modulation after simultaneously recorded GPi bursts or pauses. Detection thresholds were set to the 2.5^{th} and 97.5^{th} percentile of the baseline before each event. If the average TA within 0-100 ms after the event crossed one of the thresholds, the TA was assigned to be 'decreasing' or 'increasing', respectively. Finally, we computed a population average of all cross-correlations between GPi pause and GPi burst offset times, both smoothed with a Gaussian density of standard deviation $\sigma = 10$ ms.

Statistical testing

For each analysis relating to cell-pair interactions (Fig. 4 and 5, Table 2), we computed surrogate data as described above. Permutations were done 400 times and each set of shuffled data was processed identically to unshuffled data. The resulting 400 surrogate data sets were then used as a control distribution of which the 2.5^{th} and the 97.5^{th} percentile were taken as limits of the 95% confidence interval. For analyses that involve multiple comparisons, the confidence intervals were shifted such that in total, 5% of shuffled controls became significant for any comparison.

Differences in distributions were tested by comparison of Kolmogorov-Smirnov (KS)-statistics. We computed the one-sided KS-statistic comparing the empirically obtained distribution to 399 control distributions ('test statistic') as well as the one-sided KS-statistic of each of 400 the control distributions compared to the remaining 399 control distributions (400 'control statistics'). If the test statistic was larger than the 95th percentile of the control statistics, we concluded that the obtained distribution was significantly right-shifted relative to the control distribution.

Simulations

Custom Matlab code was written to generate N (N=5, 20, 100) simulated GPi spike trains of duration 100 sec, with ISIs stochastically selected from a gamma distribution, with firing rate 70 Hz for each train, and with a specified level c of spike time correlation between each pair of trains (c=0, 0.1, 0.2, 0.3, 0.4). Spike times from the collection of all GPi trains were converted into a single synaptic conductance time series. Specifically, each spike was convolved with an exponential kernel with decay time constant 5 msec, scaled to have total area 7 units. The conductance time series computed from all N GPi neurons, multiplied by a factor of 0.03 so that individual inputs near resting potential induce membrane variations of 1-2 mV and then divided by N for normalization, was taken as input in the simulation of 100 sec of activity of a model thalamocortical relay neuron (TC) used in past studies [103], performed in the freely available software XPPAUT [104]. TC spike times were computed as times of voltage crossing through a threshold of -20 mV. Using the XCOV function in Matlab, pairwise cross-correlations were computed between the TC spike times and those of 5 randomly selected GPi spike trains for each trial. A total of 20 cross-correlations, from 4 separate simulations, were averaged for each (N,c) pair. From each averaged cross-correlation, the value of maximum magnitude was computed and the time lag at which this maximum occurred was determined.

Average cross-correlations in the interval [0,10ms] were compared to a linear approximation of the simulations motivated as follows. Let $s_j(t)$ be a representation of the spike train of GPi neuron j=1, …, N. For a discrete time representation, this is a binarized spike train; in continuous time, it is a sum of Dirac delta functions. The synaptic conductance to the single VLa neuron induced by the whole GPi population can be written as

$$g(t) = K * \sum_{j}^{N} J\, s_j(t)$$

where $*$ denotes convolution and $K(t)$ is a kernel representing the postsynaptic conductance waveform. To keep the total conductance fixed as N changes, the synaptic weights were chosen as $\mathrm{J} = \mathrm{b}/\mathrm{N}$ for a constant $\mathrm{b} < 0$. The cross-correlation between a single GPi spike train and the total synaptic conductance is the cross-correlation between the two time-series where one has been translated in time by lag τ. Omitting the explicit time translation, we can write the GPi-VLa cross-correlation at any fixed lag τ as

$$\frac{cov(s_k, g)}{\sigma^2}$$

$$= \frac{1}{\sigma^2} cov\left(s_k, K * \sum_{j=1}^{N} J\, s_j(t) \right)$$

$$= \frac{b\, K}{\sigma^2 N} * \sum_{j=1}^{N} cov\left(s_k, s_j\right)$$

$$= \frac{b\, K}{\sigma^2 N} * \left(\sum_{j \neq k}^{N} cov\left(s_j, s_k\right) + cov\left(s_j, s_j\right) \right)$$

$$= \frac{b\, K}{N} * \left((N-1)c + 1\right)$$

$$= a\, \frac{\left((N-1)c + 1\right)}{N}$$

where σ^2 is the auto-covariance of each s_j, $c = cov(s_j, s_k)/\sigma^2$ is the cross-correlation between GPi spike trains at time lag τ, and $a = b \int_{-\infty}^{\infty} K(t)dt\ \ is$ a constant. The cross-correlation between model GPi spike trains and synaptic conductance is mapped non-linearly to the cross-correlation between GPi spike trains and the VLa spike train. However, when correlations are

small, a linear approximation to the transfer of cross-correlation from input to output is accurate [105; 106]. Hence, the cross-correlation between a model GPi spike train and the VLa spike train at any fixed lag τ is approximately propotional to $\frac{N-1}{N}c + 1/N$ at least when correlations are weak. The linear approximation was fitted to the data by a least squares fit.

Bibliography

[1] Goldberg, J.H., Farries, M.A. & Fee, M.S., 2012. Integration of cortical and pallidal inputs in the basal ganglia-recipient thalamus of singing birds. *Journal of Physiology*, 108(5), pp.1403-1429, DOI: 10.1152/jn.00056.2012.

[2] Goldberg, J.H., Farries, M.A. & Fee, M.S., 2013. Basal ganglia output to the thalamus: still a paradox. *Trends in Neurosciences*, 36(12), pp.695–705, DOI: 10.1016/j.tins.2013.09.001.

[3] Anderson, C.J., Sheppard, D.T., Huynh, R., Nesterovich Anderson, D., Polar, C.A., & Dorval, A.D., 2015. Subthalamic deep brain stimulation reduces pathological information transmission to the thalamus in a rat model of parkinsonism. *Frontiers in Neural Circuits*, 9, p.31, DOI: 10.3389/fncir.2015.00031.

[4] Bosch-Bouju, C., Smither, R. A., Hyland, B. I., & Parr-Brownlie, L. C., 2014a. Reduced reach-related modulation of motor thalamus neural activity in a rat model of Parkinson's disease. *Journal of Neuroscience*, 34(48), pp.15836–15850, DOI: 10.1523/JNEUROSCI.0893-14.2014.

[5] Kammermeier, S., Pittard, D., Hamada, I., & Wichmann, T., 2016. Effects of high-frequency stimulation of the internal pallidal segment on neuronal activity in the thalamus in parkinsonian monkeys. *Journal of Neurophysiology*, 116(6), pp.2869-288, DOI: 10.1152/jn.00104.2016.

[6] Ueki, A., 1983. The mode of nigro-thalamic transmission investigated with intracellular recording in the cat. Experimental Brain Research, 49(1), pp.116-124, DOI: 10.1007/bf00235546.

[7] Penney Jr, J. B., & Young, A. B. 1981. GABA as the pallidothalamic neurotransmitter: implications for basal ganglia function. *Brain Research*, 1(23), pp.195-199, DOI: 10.1016/0006-8993(81)90693-4.

[8] Kuramoto, E., Fujiyama, F., Nakamura, K. C., Tanaka, Y., Hioki, H., & Kaneko, T. 2011. Complementary distribution of glutamatergic cerebellar and GABAergic basal ganglia afferents to the rat motor thalamic nuclei. *European Journal of Neuroscience*, 33(1), pp.95-109, DOI: 10.1111/j.1460-9568.2010.07481.x.

[9] DeLong, M. R., 1971. Activity of pallidal neurons during movement. *Journal of Neurophysiology*, 34(3), pp.414-427, DOI: 10.1152/jn.1971.34.3.414.

[10] Bodor, Á. L., Giber, K., Rovó, Z., Ulbert, I., & Acsády, L. 2008. Structural correlates of efficient GABAergic transmission in the basal ganglia–thalamus pathway. *Journal of Neuroscience*, 28(12), pp.3090-3102, DOI: 10.1523/JNEUROSCI.5266-07.2008.

[11] Ilinsky, I. A., Yi, H., & Kultas□Ilinsky, K. 1997. Mode of termination of pallidal afferents to the thalamus: a light and electron microscopic study with anterograde tracers and

immunocytochemistry in Macaca mulatta. *Journal of Comparative Neurology*, 386(4), pp.601-612, DOI: 10.1002/(sici)1096-9861(19971006)386:4<601::aid-cne6>3.0.co;2-6.

[12] Albin, R. L., Young, A. B., & Penney, J. B., 1989. The functional anatomy of basal ganglia disorders. *Trends in Neurosciences*, 12(10), pp.366-375, DOI: 10.1016/0166-2236(89)90074-x.

[13] Hikosaka, O. 2007. GABAergic output of the basal ganglia. *Progress in Brain Research*, 160, pp.209-226, DOI: 10.1016/S0079-6123(06)60012-5.

[14] Chevalier, G. & Deniau, J.M., 1990. Disinhibition as a basic process in the expression of striatal functions. *Trends in Neurosciences*, 13(7), pp.277–280, DOI: 10.1016/0166-2236(90)90109-n.

[15] Deniau, J.M. & Chevalier, G., 1985. Disinhibition as a basic process in the expression of striatal functions. II. The striato-nigral influence on thalamocortical cells of the ventromedial thalamic nucleus. *Brain Research*, 334(2), pp.227–233, DOI: 10.1016/0006-8993(85)90214-8.

[16] Nambu, A., 2004. A new dynamic model of the cortico-basal ganglia loop. *Progress in Brain Research*, 143, pp.461–466, DOI: 10.1016/S0079-6123(03)43043-4.

[17] Nambu, A., Yoshida, S. & Jinnai, K., 1991. Movement-related activity of thalamic neurons with input from the globus pallidus and projection to the motor cortex in the monkey. *Experimental Brain Research*, 84(2), pp.279–284, DOI: 10.1007/bf00231447.

[18] Person, A.L. & Perkel, D.J., 2007. Pallidal neuron activity increases during sensory relay through thalamus in a songbird circuit essential for learning. *The Journal of Neuroscience*, 27(32), pp.8687–8698, DOI: 10.1523/JNEUROSCI.2045-07.2007.

[19] Bosch-Bouju, C., Hyland, B.I. & Parr-Brownlie, L.C., 2014b. Motor thalamus integration of cortical, cerebellar and basal ganglia information: implications for normal and parkinsonian conditions. *Frontiers in Computational Neuroscience*, 7, p.163, DOI: 10.3389/fncom.2013.00163.

[20] Person, A.L. & Perkel, D.J., 2005. Unitary IPSPs drive precise thalamic spiking in a circuit required for learning. *Neuron*, 46(1), pp.129–140, DOI: 10.1016/j.neuron.2004.12.057.

[21] Leblois, A., Bodor, Á. L., Person, A. L., & Perkel, D. J., 2009. Millisecond timescale disinhibition mediates fast information transmission through an avian basal ganglia loop. *Journal of Neuroscience*, 29(49), pp.15420-15433, DOI: 10.1523/JNEUROSCI.3060-09.2009.

[22] Kim, J., Kim, Y., Nakajima, R., Shin, A., Jeong, M., Park, A. H., Jeong, Y., Jo, S., Yang, S., Park, H., Cho, S., Cho, K., Shim, I., Chung, J. H., Paik, S., Augustine, G. J., & Kim, D., 2017. Inhibitory basal ganglia inputs induce excitatory motor signals in the thalamus. *Neuron*, 95(5), pp.1181-1196, DOI: 10.1016/j.neuron.2017.08.028.

[23] Anderson, M. E., Inase, M., Buford, J., & Turner, R. S., 1993. Movement and preparatory activity of neurons in pallidal-receiving areas of the monkey thalamus. *Role of the Cerebellum and Basal Ganglia in Voluntary Movement, Excerpta Medica*, Amsterdam, pp.163-170.

[24] Inase, M., Buford, J.A. & Anderson, M.E., 1996. Changes in the control of arm position, movement, and thalamic discharge during local inactivation in the globus pallidus of the monkey. *Journal of Neurophysiology*, 75(3), pp.1087-1104, DOI: 10.1152/jn.1996.75.3.1087.

[25] Goldberg, J.H. & Fee, M.S., 2012. A cortical motor nucleus drives the basal ganglia-recipient thalamus in singing birds. *Nature Neuroscience*, 15(4), pp.620–627, DOI: 10.1038/nn.3047.

[26] Nambu, A., 2008. Seven problems on the basal ganglia. *Current Opinion in Neurobiology*, 18(6), pp.595-604, DOI: 10.1016/j.conb.2008.11.001.

[27] Turner, R.S. & Desmurget, M., 2010. Basal ganglia contributions to motor control: a vigorous tutor. *Current Opinion in Neurobiology*, 20(6), pp.704–716, DOI: 10.1016/j.conb.2010.08.022.

[28] Anderson, M. E., & Horak, F. B., 1985. Influence of the globus pallidus on arm movements in monkeys. III. Timing of movement-related information. *Journal of Neurophysiology*, 54(2), pp.433-448, DOI: 10.1152/jn.1985.54.2.433.

[29] Brotchie, P., Iansek, R. & Horne, M.K., 1991. Motor function of the monkey globus pallidus. 2. Cognitive aspects of movement and phasic neuronal activity. *Brain: A Journal of Neurology*, 114(4), pp.1685–1702, DOI: 10.1093/brain/114.4.1685.

[30] Mitchell, S. J., Richardson, R. T., Baker, F. H., & DeLong, M. R. 1987. The primate globus pallidus: Neuronal activity related to direction of movement. *Exp Brain Res*, 68, pp.491-505, DOI: 10.1007/bf00249793.

[31] Mink, J.W. & Thach, W.T., 1991. Basal ganglia motor control. II. Late pallidal timing relative to movement onset and inconsistent pallidal coding of movement parameters. *Journal of Neurophysiology*, 65(2), pp.301–329, DOI: 10.1152/jn.1991.65.2.301.

[32] Turner, R.S. & Anderson, M.E., 1997. Pallidal discharge related to the kinematics of reaching movements in two dimensions. *Journal of Neurophysiology*, 77(3), pp.1051–1074, DOI: 10.1152/jn.1997.77.3.1051.

[33] van Donkelaar, P., Stein, J. F., Passingham, R. E., & Miall, R. C., 1999. Neuronal activity in the primate motor thalamus during visually triggered and internally generated limb movements. *Journal of Neurophysiology*, 82(2), pp.934-945, DOI: 10.1152/jn.1999.82.2.934.

[34] Anderson, M. E., & Turner, R. S., 1991. Activity of neurons in cerebellar-receiving and pallidal-receiving areas of the thalamus of the behaving monkey. *Journal of Neurophysiology*, 66(3), pp.879-893, DOI: 10.1152/jn.1991.66.3.879.

[35] Luo, M., & Perkel, D. J., 1999. A GABAergic, strongly inhibitory projection to a thalamic nucleus in the zebra finch song system. *Journal of Neuroscience*, 19(15), pp.6700-6711, DOI: PMC6782801.

[36] Parent, M., Lévesque, M., & Parent, A., 2001. Two types of projection neurons in the internal pallidum of primates: single□axon tracing and three-dimensional reconstruction. *Journal of Comparative Neurology*, 439(2), pp.162-175, DOI: 10.1002/cne.1340.

[37] Graybiel, A.M., Aosaki, T., Flaherty, A. & Kimura, A., 1994. The basal ganglia and adaptive motor control. *Science*, 265(5180), pp.1826–1831, DOI: 10.1126/science.8091209.

[38] Alexander, G. E., Crutcher, M. D., & DeLong, M. R., 1991. Basal ganglia-thalamocortical circuits: parallel substrates for motor, oculomotor, “prefrontal” and “limbic” functions. *Progress in Brain Research*, 85, pp.119-146, DOI: 10.1016/S0079-6123(08)62678-3.

[39] Buhusi, C.V. & Meck, W.H., 2005. What makes us tick? Functional and neural mechanisms of interval timing. *Nature Reviews Neuroscience*, 6(10), pp.755–765, DOI: 10.1038/nrn1764.

[40] Mink, J.W., 1996. The basal ganglia: focused selection and inhibition of competing motor programs. *Progress in Neurobiology*, 50(4), pp.381–425, DOI: 10.1016/s0301-0082(96)00042-1.

[41] Redgrave, P., Prescott, T. J., & Gurney, K., 1999. The basal ganglia: a vertebrate solution to the selection problem? *Neuroscience*, 89(4), pp.1009-1023, DOI: 10.1016/s0306-4522(98)00319-4.

[42] Barter, J. W., Li, S., Sukharnikova, T., Rossi, M. A., Bartholomew, R. A., & Yin, H. H., 2015. Basal ganglia outputs map instantaneous position coordinates during behavior. *Journal of Neuroscience*, 35(6), pp.2703-2716, DOI: 10.1523/JNEUROSCI.3245-14.2015.

[43] DeLong, M.R. & Wichmann, T., 2007. Circuits and circuit disorders of the basal ganglia. *Archives of Neurology*, 64(1), pp.20–24, DOI: 10.1001/archneur.64.1.20.

[44] Yttri, E. A., & Dudman, J. T., 2016. Opponent and bidirectional control of movement velocity in the basal ganglia. *Nature*, 533(7603), p.402, DOI: 10.1038/nature17639.

[45] Thura, D., & Cisek, P., 2017. The basal ganglia do not select reach targets but control the urgency of commitment. *Neuron*, 95(5), pp.1160-1170, DOI: 10.1016/j.neuron.2017.07.039.

[46] Rye, D. B., Lee, H. J., Saper, C. B., & Wainer, B. H., 1988. Medullary and spinal efferents of the pedunculopontine tegmental nucleus and adjacent mesopontine tegmentum in the rat. *Journal of Comparative Neurology*, 269(3), pp.315-341.

[47] Mena-Segovia, J., Bolam, J. P., & Magill, P. J., 2004. Pedunculopontine nucleus and basal ganglia: distant relatives or part of the same family? *Trends in Neurosciences*, 27(10), 585-588, DOI: 10.1016/j.tins.2004.07.009.

[48] Franco, V., & Turner, R. S., 2012. Testing the contributions of striatal dopamine loss to the genesis of parkinsonian signs. *Neurobiology of Disease*, 47(1), pp.114-125, DOI: 10.1016/j.nbd.2012.03.028.

[49] Zimnik, A. J., Nora, G. J., Desmurget, M., & Turner, R. S., 2015. Movement-related discharge in the macaque globus pallidus during high-frequency stimulation of the subthalamic nucleus. *Journal of Neuroscience*, 35(9), pp.3978-3989, DOI: 10.1523/JNEUROSCI.4899-14.2015.

[50] Hoover, J. E., & Strick, P. L., 1993. Multiple output channels in the basal ganglia. *Science*, 259, pp.819-821, DOI: 10.1126/science.7679223.

[51] Nambu, A., Yoshida, S., & Jinnai, K., 1988. Projection on the motor cortex of thalamic neurons with pallidal input in the monkey. *Experimental Brain Research*, 71(3), pp.658-662, DOI: 10.1007/bf00248759.

[52] Tachibana, Y., Kita, H., Chiken, S., Takada, M., & Nambu, A., 2008. Motor cortical control of internal pallidal activity through glutamatergic and GABAergic inputs in awake monkeys. *European Journal of Neuroscience*, 27(1), pp.238-253, DOI: 10.1111/j.1460-9568.2007.05990.x.

[53] Galvan, A., Hu, X., Smith, Y., & Wichmann, T., 2016. Effects of optogenetic activation of corticothalamic terminals in the motor thalamus of awake monkeys. *Journal of Neuroscience*, 36(12), 3519-3530, DOI: 10.1523/JNEUROSCI.4363-15.2016.

[54] Wichmann, T. & Soares, J., 2006. Neuronal firing before and after burst discharges in the monkey basal ganglia is predictably patterned in the normal state and altered in parkinsonism. *Journal of Neurophysiology*, 95(4), pp.2120–2133, DOI: 10.1152/jn.01013.2005.

[55] Kasten, M. R. & Anderson, M. P., (2015). Self-regulation of adult thalamocortical neurons. *Journal of Neurophysiology*, 114(1), pp. 323-31, DOI: 10.1152/jn.00800.2014.

[56] Nini, A., Feingold, A., Slovin, H., & Bergman, H., 1995. Neurons in the globus pallidus do not show correlated activity in the normal monkey, but phase-locked oscillations appear in the MPTP model of parkinsonism. *Journal of Neurophysiology*, 74(4), pp.1800-1805, DOI: 10.1152/jn.1995.74.4.1800.

[57] Raz, A., Frechter-Mazar, V., Feingold, A., Abeles, M., Vaadia, E., & Bergman, H. (2001). Activity of pallidal and striatal tonically active neurons is correlated in MPTP-treated monkeys but not in normal monkeys. Journal of Neuroscience, 21(3), RC128-RC128, DOI: 10.1523/JNEUROSCI.21-03-j0006.2001

[58] Bar-Gad, I., Heimer, G., Ritov, Y. A., & Bergman, H., 2003a. Functional correlations between neighboring neurons in the primate globus pallidus are weak or nonexistent. *Journal of Neuroscience*, 23(10), pp.4012-4016, DOI: 10.1523/JNEUROSCI.23-10-04012.2003.

[59] Wilson, C. J., 2013. Active decorrelation in the basal ganglia. *Neuroscience*, 250, 467-482, DOI: 10.1016/j.neuroscience.2013.07.032.

[60] Rouiller, E. M., Tanné, J., Moret, V., Kermadi, I., Boussaoud, D., & Welker, E., 1998. Dual morphology and topography of the corticothalamic terminals originating from the primary, supplementary motor, and dorsal premotor cortical areas in macaque monkeys. *Journal of Comparative Neurology*, 396(2), pp.169-185, DOI: 10.1002/(sici)1096-9861(19980629)396:2<169::aid-cne3>3.0.co;2-z.

[61] McFarland, N. R., & Haber, S. N., 2002. Thalamic relay nuclei of the basal ganglia form both reciprocal and nonreciprocal cortical connections, linking multiple frontal cortical areas. *Journal of Neuroscience*, 22(18), pp.8117-8132, DOI: 10.1523/JNEUROSCI.22-18-08117.2002.

[62] Schmidt, R., Leventhal, D. K., Mallet, N., Chen, F., & Berke, J. D., 2013. Canceling actions involves a race between basal ganglia pathways. Nature Neuroscience, 16(8), 1118-1124, DOI: 10.1038/nn.3456

[63] Guo, Z. V., Inagaki, H. K., Daie, K., Druckmann, S., Gerfen, C. R., & Svoboda, K. 2017. Maintenance of persistent activity in a frontal thalamocortical loop. Nature, 545(7653), 181-186, DOI: 10.1038/nature22324

[64] Georgopoulos, A. P., DeLong, M. R., & Crutcher, M. D., 1983. Relations between parameters of step-tracking movements and single cell discharge in the globus pallidus and subthalamic nucleus of the behaving monkey. Journal of Neuroscience, 3(8), 1586-1598, DOI: 10.1523/JNEUROSCI.03-08-01586.1983

[65] Meyer□Luehmann, M., Thompson, J. F., Berridge, K. C., & Aldridge, J. W. (2002). Substantia nigra pars reticulata neurons code initiation of a serial pattern: implications for natural action sequences and sequential disorders. European Journal of Neuroscience, 16(8), 1599-1608, DOI: 10.1046/j.1460-9568.2002.02210.x

[66] Palm, G., Aertsen, A. M. H. J., & Gerstein, G. L., 1988. On the significance of correlations among neuronal spike trains. *Biological Cybernetics*, 59(1), pp.1-11, DOI: 10.1007/bf00336885.

[67] Parent, M., & Parent, A., 2004. The pallidofugal motor fiber system in primates. *Parkinsonism & Related Disorders*, 10(4), 203-211, DOI: 10.1016/j.parkreldis.2004.02.007.

[68] Cohen, M. R., & Kohn, A., 2011. Measuring and interpreting neuronal correlations. *Nature Neuroscience*, 14(7), p.811, DOI: 10.1038/nn.2842.

[69] Chan, V., Starr, P. A., & Turner, R. S., 2011. Bursts and oscillations as independent properties of neural activity in the parkinsonian globus pallidus internus. *Neurobiology of disease*, 41(1), pp.2-10, DOI: 10.1016/j.nbd.2010.08.012.

[70] Elias, S., Joshua, M., Goldberg, J. A., Heimer, G., Arkadir, D., Morris, G., & Bergman, H., 2007. Statistical properties of pauses of the high-frequency discharge neurons in the external segment of the globus pallidus. *Journal of Neuroscience*, 27(10), 2525-2538, DOI: 10.1523/JNEUROSCI.4156-06.2007.

[71] Svennilson, E., Torvik, A., Lowe, R., & Leksell, L., 1960. Treatment of parkinsonism by stereotactic thermolesions in the pallidal region. A clinical evaluation of 81 cases. *Acta Psychiatrica Scandinavica*, 35(3), 358-377, DOI: 10.1111/j.1600-0447.1960.tb07606.x.

[72] Baron, M. S., Vitek, J. L., Green, J., Kaneoke, Y., Hashimoto, T., Turner, R. S., Woodard, J. L., Cole, S. A., McDonald, W. M., & DeLong, M. R. 1996. Treatment of advanced Parkinson's disease by posterior GPi pallidotomy: 1□year results of a pilot study. *Annals of Neurology: Official Journal of the American Neurological Association and the Child Neurology Society*, 40(3), pp.355-366, DOI: 10.1002/ana.410400305.

[73] Cersosimo, M. G., Raina, G. B., Piedimonte, F., Antico, J., Graff, P., & Micheli, F. E., 2008. Pallidal surgery for the treatment of primary generalized dystonia: long-term follow-up. *Clinical neurology and neurosurgery*, 110(2), pp.145-150, DOI: 10.1016/j.clineuro.2007.10.003.

[74] Obeso, J. A., Jahanshahi, M., Alvarez, L., Macias, R., Pedroso, I., Wilkinson, L., Pavon, N., Day, B., Pinto, S., Rodriguez-Oroz, M. C., Tejeiro, J., Artieda, J., Talleli, P., Swayne, O., Rodriguez, R., Bhatia, K., Rodriguez-Diaz, M., Lopez, G., Guridi, J., Rothwell, J.C. 2009. What can man do without basal ganglia motor output? The effect of combined unilateral subthalamotomy and pallidotomy in a patient with Parkinson's disease. *Experimental Neurology*, 220(2), pp.283-292, DOI: 10.1016/j.expneurol.2009.08.030.

[75] Desmurget, M., & Turner, R. S., 2008. Testing basal ganglia motor functions through reversible inactivations in the posterior internal globus pallidus. *Journal of Neurophysiology*, 99(3), pp.1057-1076, DOI: 10.1152/jn.01010.2007.

[76] Desmurget, M., & Turner, R. S., 2010. Motor sequences and the basal ganglia: kinematics, not habits. *Journal of Neuroscience*, 30(22), 7685-7690, DOI: 10.1523/JNEUROSCI.0163-10.2010.

[77] Piron, C., Kase, D., Topalidou, M., Goillandeau, M., Orignac, H., N'Guyen, T. H., Rougier, N. & Boraud, T., 2016. The globus pallidus pars interna in goal-oriented and routine behaviors: Resolving a long-standing paradox. *Movement disorders*, 31(8), pp.1146-1154, DOI: 10.1002/mds.26542.

[78] Horak, F.B. & Anderson, M.E., 1984. Influence of globus pallidus on arm movements in monkeys. I. Effects of kainic acid-induced lesions. *Journal of Neurophysiology*, 52(2), pp.290–304, DOI: 10.1152/jn.1984.52.2.290.

[79] Jeong, M., Kim, Y., Kim, J., Ferrante, D. D., Mitra, P. P., Osten, P., & Kim, D., 2016. Comparative three-dimensional connectome map of motor cortical projections in the mouse brain. *Scientific reports*, 6, 20072.

[80] Prasad, J. A., Carroll, B. J., & Sherman, S. M. (2020). Layer 5 corticofugal projections from diverse cortical areas: variations on a pattern of thalamic and extra-thalamic targets. *Journal of Neuroscience*, , 40 (30) 5785-5796; DOI: 10.1523/JNEUROSCI.0529-20.2020

[81] Bokor H, Hadinger N, & Acsady L. 2016. Efficient cortical control of basal ganglia recipient motor thalamus. *SfN Annual Meeting Abstracts*.

[82] Catanese, J., & Jaeger, D., 2020. Nigro-Thalamic Projection Controls Timing of Action Initiation. *bioRxiv*., DOI: 10.1101/2020.01.12.903500

[83] McCairn, K. W., & Turner, R. S., 2009. Deep brain stimulation of the globus pallidus internus in the parkinsonian primate: local entrainment and suppression of low-frequency oscillations. *Journal of Neurophysiology*, 101(4), pp.1941-1960, DOI: 10.1152/jn.91092.2008.

[84] Brown, J., Pan, W. X., & Dudman, J. T. 2014. The inhibitory microcircuit of the substantia nigra provides feedback gain control of the basal ganglia output. *eLife*, 3, e02397, DOI: 10.7554/eLife.02397

[85] Bar-Gad, I., Morris, G., & Bergman, H., 2003b. Information processing, dimensionality reduction and reinforcement learning in the basal ganglia. *Progress in neurobiology*, 71(6), pp.439-473, DOI: 10.1016/j.pneurobio.2003.12.001.

[86] Wongmassang, W., Hasegawa, T., Chiken, S., & Nambu, A, 2020. Weakly correlated activity of pallidal neurons in behaving monkeys. *European Journal of Neuroscience*, DOI: 10.1111/ejn.14903

[87] Nevet, A., Morris, G., Saban, G., Arkadir, D., & Bergman, H. 2007. Lack of spike-count and spike-time correlations in the substantia nigra reticulata despite overlap of neural responses. *Journal of neurophysiology*, 98(4), 2232-2243, DOI: 10.1152/jn.00190.2007

[88] Higgs, M. H., & Wilson, C. J. 2016. Unitary synaptic connections among substantia nigra pars reticulata neurons. *Journal of neurophysiology*, 115(6), 2814-2829, DOI: 10.1152/jn.00094.2016

[89] Kao, M. H., Doupe, A. J., & Brainard, M. S., (2005). Contributions of an avian basal ganglia–forebrain circuit to real-time modulation of song. *Nature*, 433(7026), p.638, DOI: 10.1038/nature03127.

[90] Kojima, S., Kao, M. H., Doupe, A. J., & Brainard, M. S., 2018. The avian basal ganglia are a source of rapid behavioral variation that enables vocal motor exploration. *Journal of Neuroscience*, 38(45), pp.9635-9647, DOI: 10.1523/JNEUROSCI.2915-17.2018.

[91] Sheth, S. A., Abuelem, T., Gale, J. T., & Eskandar, E. N., 2011. Basal ganglia neurons dynamically facilitate exploration during associative learning. *Journal of Neuroscience*, 31(13), pp.4878-4885, DOI: 10.1523/JNEUROSCI.3658-10.2011.

[92] Ashby, F. G., Turner, B. O., & Horvitz, J. C., 2010. Cortical and basal ganglia contributions to habit learning and automaticity. *Trends in cognitive sciences*, 14(5), pp.208-215, DOI: 10.1016/j.tics.2010.02.001.

[93] Yoshida, S. I., Nambu, A., & Jinnai, K., 1993. The distribution of the globus pallidus neurons with input from various cortical areas in the monkeys. *Brain Research*, 611(1), pp.170-174, DOI: 10.1016/0006-8993(93)91791-p.

[94] Miocinovic, S., Zhang, J., Xu, W., Russo, G. S., Vitek, J. L., & McIntyre, C. C., 2007. Stereotactic neurosurgical planning, recording, and visualization for deep brain stimulation in non-human primates. *Journal of Neuroscience Methods*, 162(1-2), pp.32-41, DOI: 10.1016/j.jneumeth.2006.12.007.

[95] Turner, R., & DeLong, M., 2000. Corticostriatal activity in primary motor cortex of the macaque. *Journal of Neuroscience*, 20(18), pp.7096-7108, DOI: 10.1523/JNEUROSCI.20-18-07096.2000.

[96] DeLong, M. R., 1972. Activity of basal ganglia neurons during movement. *Brain Research* 40(1), pp.127-135, DOI: 10.1016/0006-8993(72)90118-7.

[97] Buford, J. A., Inase, M., & Anderson, M. E., 1996. Contrasting locations of pallidal-receiving neurons and microexcitable zones in primate thalamus. *Journal of neurophysiology*, 75(3), pp.1105-1116, DOI: 10.1152/jn.1996.75.3.1105.

[98] Vitek, J. L., Ashe, J., DeLong, M. R., & Kaneoke, Y., 1996. Microstimulation of primate motor thalamus: somatotopic organization and differential distribution of evoked motor responses among subnuclei. *Journal of Neurophysiology*, 75(6), pp.2486-2495, DOI: 10.1152/jn.1996.75.6.2486.

[99] Alexander, G. E., & Crutcher, M. D., 1990. Preparation for movement: neural representations of intended direction in three motor areas of the monkey. *Journal of Neurophysiology*, 64(1), pp.133-150, DOI: 10.1152/jn.1990.64.1.133.

[100] Amarasingham, A., Harrison, M. T., Hatsopoulos, N. G., & Geman, S., 2011. Conditional modeling and the jitter method of spike resampling. *Journal of Neurophysiology*, 107(2), pp.517-531, DOI: 10.1152/jn.00633.2011.

[101] Liu, S., Gu, Y., DeAngelis, G. C., & Angelaki, D. E., 2013. Choice-related activity and correlated noise in subcortical vestibular neurons. *Nature Neuroscience*, 16(1), 89, DOI: 10.1038/nn.3267.

[102] Legéndy, C.R. & Salcman, M., 1985. Bursts and recurrences of bursts in the spike trains of spontaneously active striate cortex neurons. *Journal of Neurophysiology*, 53(4), pp.926–939, DOI: 10.1152/jn.1985.53.4.926.

[103] Cleary, D. R., Raslan, A. M., Rubin, J. E., Bahgat, D., Viswanathan, A., Heinricher, M. M., & Burchiel, K. J., 2012. Deep brain stimulation entrains local neuronal firing in human globus pallidus internus. *Journal of Neurophysiology*, 109(4), 978-987, DOI: 10.1152/jn.00420.2012.

[104] Ermentrout, B., 2002. Simulating, analyzing, and animating dynamical systems: a guide to XPPAUT for researchers and students (Vol. 14). *SIAM*, Philadelphia, PA, ISBN: 978-0-89871-506-4.

[105] Lindner, B., Doiron, B., & Longtin, A., 2005. Theory of oscillatory firing induced by spatially correlated noise and delayed inhibitory feedback. *Physical Review E*, 72(6), 061919, DOI: 10.1103/PhysRevE.72.061919.

[106] Shea-Brown, E., Josić, K., de La Rocha, J., & Doiron, B., 2008. Correlation and synchrony transfer in integrate-and-fire neurons: basic properties and consequences for coding. *Physical Review Letters*, 100(10), 108102.

Tables

	GPi			***VLa***		
	NHP G	NHP I	Total	NHP G	NHP I	Total
Number of Units	105	104	209	66	119	185
Mean rate at rest [sp/s (SD)]	70.8 (26.0)	69.4 (29.9)	**70.1 (27.9)**	14.8 (10.8)	14.2 (11.4)	**13.5 (10.5)**
Action potential width [msec min-to-max (SD)]	0.24 (0.06)	0.24 (0.11)	**0.24 (0.09)**	0.46 (0.22)	0.53 (0.19)	**0.50 (0.21)**
Movement-responsive neurons [number (%)]	102 (97)	104 (100)	206 (99)	58 (87.9)	105 (88.2)	163 (88.1)
Mvt-related Responses	187	201	388	110	216	326
Increase only	109	80	**189 (48.7)**	81	132	**213 (65.3)**
Decrease only	33	37	**70 (18.0)**	20	57	**77 (23.6)**
Polyphasic increase first	29	37	**66 (17.0)**	5	13	**18 (5.5)**
Polyphasic decrease first [number (%)]	16	47	**63 (16.2)**	4	14	**18 (5.5)**
*Increases (proportion of all detected changes *)*	66.4% (154/232)	57.5% (164/285)	**61.5% (318/517)**	75.6% (90/119)	65.4% (159/243)	**68.8% (249/362)**
Mean integrated change [sp (SD)×10^3]	4.38 (10.0)	3.41 (11.4)	**3.89 (10.7)**	3.24 (7.07)	0.96 (3.61)	**1.75 (5.19)**
Response latencies (msec relative to reach onset)						
Increases (medians)	−77.5	−74	−76	−87.5	−88.5	−88
Decreases (medians)	31	−52.5	**−31.5**	−117	−89	**−95.5**

Table 1: Database and basic properties of neurons

Bold: significant difference between GPi and VLa neurons by Wilcoxon rank sum or chi-square tests.

* For proportion of increases, biphasic responses are counted twice to account for the simultaneous presence of an increase and decrease in firing.

Table 2: Cell-pair interactions between GPi and VLa

	Cross-correlations	*Noise correlations*	*Burst/pause influences*
Number of GPi-VLa pairs	Whole recordings: 427 During rest: 183 During movement: 172	During rest: 332 During movement: 372	Burst onsets: 163 Burst offsets: 167 Pause onsets: 153
Fraction of significant pairs (total number)	Whole recordings: 3.5% (15) During rest: 2.2% (4) During movement: 5.2% (9)	During rest: 5.4% (18) 44% positive (8) 56% negative (10) During movement: 7.2% (27) 41% positive (11) 59% negative (16)	Burst onsets: 11.6% (19) 74% decreases (14) 26% increases (5) Burst offsets: 7.8% (13) 77% decreases (10) 23% increases (3) Pause onsets: 8.5% (13) 69% decreases (9) 31% increases (4)

Significant Cross-correlations: pairs with absolute CCF peaks exceeding 95% of the control distribution.

Significant noise correlations: pairs with maximum/minimum correlations larger/smaller than 97.5% of the control distribution.

Significant burst/pause influences: pairs with average VLa firing rates 0-100ms after GPi burst/pause onset/offset above/below 97.5% of their baseline firing.

Table 3: Overview

Relationships between GPi and VLa
Hypothesized versus Observed

	Gating [15; 41]	**Rebound** [18; 22]	**Observed**
Incidence of increase- vs. decrease-type responses	Inverted. GPi increases proportional to VLa decreases	Direct. GPi increases proportional to VLa increases	Direct. Similar rates of increases found in GPi and VLa (see Table 1)
Timing of movement-related responses	GPi leads VLa by ~2 ms	GPi leads VLa by ~100 ms	GPi lags VLa by ~43 ms (see Fig. 3A)
GPi-VLa spike-spike cross correlation functions (CCFs)	Negative CCF peaks at short latency in sub-population of pairs	CCF peaks negative at short latency followed by positive at long latency.	CCF peaks are rare (at noise rate). No net bias toward negative or positive peaks. (see Fig. 4A-F and Table 2)
GPi-VLa firing rate correlations (noise correlations, "NCs")	Negative NCs are larger and/or more common	Positive NCs are larger and/or more common	Significant NCs are rare w/no net bias toward positive or negative relationships (see Fig. 4G-H and Table 2)
VLa firing rate (FR) following burst in GPi firing	VLa FR decreases at short latency (~2 ms)	VLa FR decreases following burst onset	Long-lasting (>200 ms) VLa decrease w/pause part of GPi burst-pause complex (see Fig. 5)
VLa firing rate (FR) following pauses in GPi firing	VLa FR increases at short latency (~2 ms)	VLa FR increases at short latency	

Supporting Information S1 Figure: *The locations of all GPi and VLa single-units included in the database (black tick marks) are plotted on parasagittal sections 1 mm intervals separately for animals G and I. Green bars indicate the locations of SCP-responsive VLp neurons. Gray bars indicate the locations of activity characteristic of the reticular nucleus of the thalamus. Line drawings of nuclear boundaries were taken from a standard atlas that was then warped to align with the structural MRIs and microelectrode mapping results from individual animals.*

Supporting Information S2 Figure: *Both animals performed the behavioral task in a highly stereotyped fashion with short reaction times and movement durations. A. Reaction times did not differ significantly between the two animals (NHP G vs. NHP I) or between the two reach directions (Left vs. Right target location). B. Movement durations were longer for reaches to the right target than to the left target. NHP G moved more slowly overall compared with NHP I.*

Data and code to reproduce this figure can be found in https://doi.org/10.5061/dryad.0cfxpnvxm (FigS2.m).

Supporting Information S3 Figure: *Reach-related modulations in muscle activity began well in advance of the mechanically-detected onset of movement. Rectified low-pass filtered EMG from proximal arm muscles was collected during a subset of data collection sessions (n = 667 and 476 trials in NHPs G and I, respectively). Signals from each muscle were averaged across trials separately for reaches to left and right targets (blue and green traces, respectively). The width of each trace reflects the SEM. The earliest reach-related modulation in EMG in both animals consisted of a reduction in Triceps resting activity followed soon thereafter by increases in two agonist muscles (Anterior Deltoid and Biceps; red vertical dashed lines), which occurred at similar pre-movement timing in both animals (-123 and -135 ms in NHPs G and I). For reference, red tick-marks at the bottom of each panel indicate the times on individual trials of Go-cue presentation and target touch at the end of the reach. EMG from Pectoralis was not available for NHP I due to poor signal quality.*

Data and code to reproduce this figure can be found in https://doi.org/10.5061/dryad.0cfxpnvxm (FigS3.m).

Supporting Information S4 Figure: *Peri-movement activity of individual single-units from GPi and VLa (left and right columns, respectively) reflecting each of the four basic forms of response (rows A-D). The panel for each single-unit shows in overlay, a mean spike-density function (black, left y-axis) and a mean interspike-interval function (gray, right y-axis), both constructed from the same underlying spike-train. The spike-density function was used to test for increases in firing rate relative to pre-go cue baseline activity (linear trend ±CI, sloped yellow lines solid and dotted, respectively). The onset time of significant increases in*

firing are indicated by vertical yellow lines. The interspike-interval function was used to test for peri-movement decreases in firing, again relative to baseline activity (linear trend ±CI, sloped blue lines). The time of onset of significant decreases in firing are indicated by vertical blue lines. Note the presence of significant increases and decreases in firing for single-units with activity classified as polyphasic.

Data and code to reproduce this figure can be found in https://doi.org/10.5061/dryad.0cfxpnvxm (FigS4.m).

***Supporting Information S5 Figure**: Performance of the response detection algorithm at detecting simulated increases versus decreases in firing rate. Curves reflect the mean (±SD) fraction of increases and decreases detected as a function of the simulated response size (expressed as percent of baseline firing rate). For GPi, the fraction of simulated responses detected was very similar for increases and decreases (red and blue curves, respectively) independent of the response size. For VLa, the algorithm was more effective at detecting decreases than increases when the simulated change in rate was relatively small (<100% of baseline). That bias disappeared for larger response sizes (>100% of baseline). Boxplots show the distributions of response in our recorded data plotted separately for increases and decreases for each cell type.*

Data and code to reproduce this figure can be found in https://doi.org/10.5061/dryad.0cfxpnvxm (FigS5.m).

***Supporting Information S6 Figure:** A. Population-level peri-movement activity did not differ between directions of movement. Population mean spike-density functions (±SEM) compiled separately for movements to left and right targets. B. The distribution of all possible pairings of the four response types in individual neurons for left and right directions of movement. Large fractions of neurons in GPi and VLa (color scale) had the same type of response for both directions of movement (denoted by colors in squares located on the diagonals of the matrices). C. Integrated changes in firing rate during the peri-movement period plotted for individual neurons for movements to left (abscissa) versus right (ordinate) targets. The polarity and magnitude of integrated changes was in general correlated between the two directions for both GPi and VLa units. Nonetheless, the peri-movement activity of many units differed significantly between left and right reaches (red symbols; 53% and 31% of units in GPi and VLa, respectively). D. The polarities of integrated firing-rate changes for left- and right-ward movements were distributed similarly for neurons in GPi and VLa. E. The overall proportions of peri-movement responses classified into the four response forms. Although the exact proportions differed somewhat between GPi and VLa populations, the overall distribution showed a similar pattern for GPi and VLa populations.*

Data and code to reproduce this figure can be found in https://doi.org/10.5061/dryad.0cfxpnvxm (FigS6_S8.m).

Supporting Information S7 Figure: *Lack of bias in response latency estimation when the detection algorithms were applied to simulated GPi and VLa responses. By design, the simulated responses began at time zero but otherwise matched the individual metrics of each empirically observed response (baseline rate, baseline variability, response magnitude and slope of response onset). The figure follows the conventions of Fig. 3. Detected onset times in GPi and VLa did not differ significantly.*

Data and code to reproduce this figure can be found in https://doi.org/10.5061/dryad.0cfxpnvxm (FigS7.m).

Supporting Information S8 Figure: *Panels A-C: Cumulative distributions of onset latencies restricted to responses in the preferred direction of units with peri-movement activity that was significantly directional. Panels D-F: Cumulative distributions of onset latencies as defined by the alternate, 10% of maximum, method. The figure follows the conventions of Fig. 3.*

*A. Comparisons of latencies of all peri-movement changes detected in GPi neurons (blue) and VLa neurons (purple). VLa responses precede GPi by a median of 28 ms. (** $p<0.001$ rank sum test)*

B. Response onset latencies of VLa increases (purple) lead GPi decreases (blue) by a median of 28.5 ms. (ns $p>0.05$ rank sum test)

C. Response onset latencies of VLa decreases (purple) lead GPi increases (blue) by a median of 29.5 ms. ($p<0.05$ rank sum test)*

*D. Comparisons of latencies of all peri-movement changes detected in GPi neurons (blue) and VLa neurons (purple). VLa responses precede GPi by a median of 41 ms. (** $p<0.001$ rank sum test)*

*E. Response onset latencies of VLa increases (purple) lead GPi decreases (blue) by a median of 65 ms. (** $p<0.001$ rank sum test)*

F. Response onset latencies of VLa decreases (purple) lead GPi increases (blue) by a median of 13.5 ms. (ns $p>0.05$ rank sum test)

Data and code to reproduce this figure can be found in https://doi.org/10.5061/dryad.0cfxpnvxm (FigS6_S8.m , Fig2_3_S8_S9.m).

Supporting Information S9 Figure: *Relation between response magnitudes and latencies is inconsistent between GPi and VLa. In GPi (blue), response magnitudes did not differ*

significantly as a function of onset latencies for either increase- or decrease-type responses (top and bottom scatter plots, respectively). In VLa (purple), response magnitudes were larger for early onset responses than for late responses. Insets: values for rho and significance from Spearman rank correlation tests.

Data and code to reproduce this figure can be found in https://doi.org/10.5061/dryad.0cfxpnvxm (Fig2_3_S8_S9.m).

Supporting Information S10 Figure: *A-C: Histograms of significant signed peak correlations. D-F: Example CCFs achieving significance. Vertical scale bars for each example indicates CCF = 0.2. G-I: Scatter plots of peak correlation values and confidence intervals.*

Data and code to reproduce this figure can be found in https://doi.org/10.5061/dryad.0cfxpnvxm (Fig4_S10to13.m).

Supporting Information S11 Figure: *Sensitivity analysis for CCFs. A-C: Cumulative histograms of measured peak correlations (black) before exclusion of pairs with $c_0 > 0.3$, minimum reliably detectable correlations c_0 (red), and upper bounds of the measured correlations c_u (green). The cutoff $c_o > 0.3$ is indicated by dashed lines. D-F: Scatter plots of measured correlations vs c_o. Significant correlations are marked red.*

Data and code to reproduce this figure can be found in https://doi.org/10.5061/dryad.0cfxpnvxm (Fig4_S10to13.m).

Supporting Information S12 Figure: *CCFs between GPi units recorded from different electrodes. The figure follows the conventions of Fig. 4. Dashed lines in panel D indicate the average CCF after exclusion of outliers.*

Data and code to reproduce this figure can be found in https://doi.org/10.5061/dryad.0cfxpnvxm (Fig4_S10to13.m).

Supporting Information S13 Figure: *Scatter plots of VLa and GPi rates for the three largest noise correlations.*

Data and code to reproduce this figure can be found in https://doi.org/10.5061/dryad.0cfxpnvxm (Fig4_S10to13.m).

Supporting Information S14 Figure: *Example GPi burst offset-triggered average firing rate in VLa (mean +/- SEM). Burst offsets correspond to time 0.*

Data and code to reproduce this figure can be found in https://doi.org/10.5061/dryad.0cfxpnvxm (Fig5_S14.m).

Fig. 1

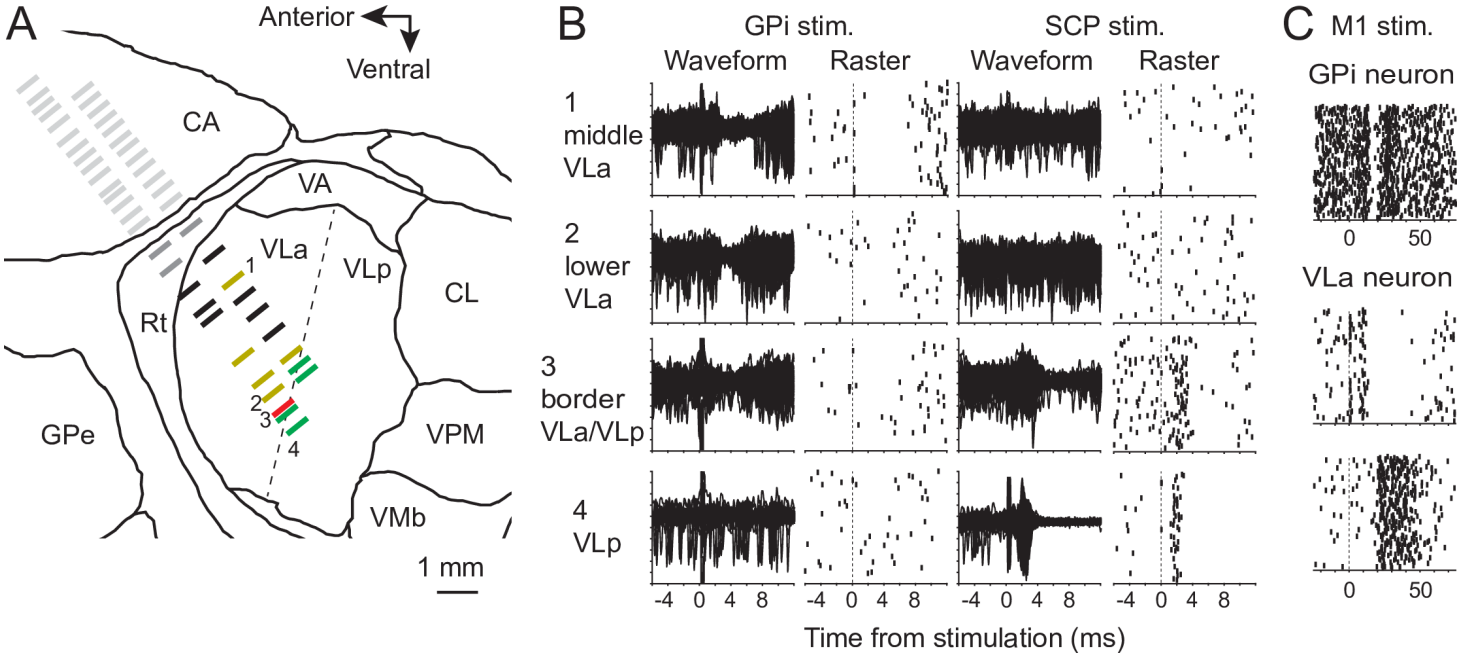
A
Anterior
Ventral
CA
VA
VLa
VLp
CL
Rt
GPe
VPM
VMb
1
2
3
4
1 mm
B
GPi stim.
SCP stim.
Waveform
Raster
Waveform
Raster
1 middle VLa
2 lower VLa
3 border VLa/VLp
4 VLp
-4 0 4 8
Time from stimulation (ms)
C
M1 stim.
GPi neuron
0 50
VLa neuron
0 50

Fig. 2

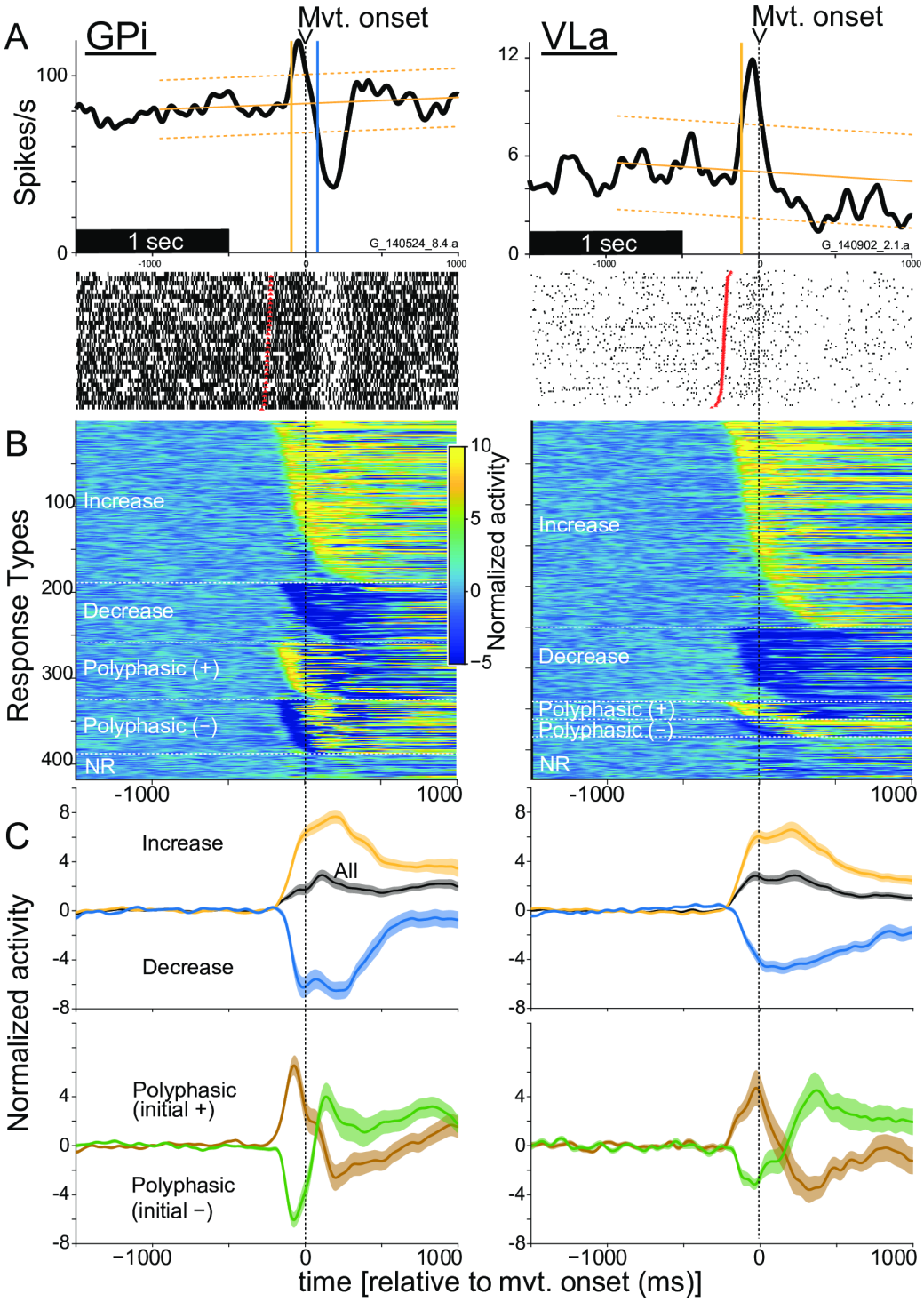
A
GPi
Mvt. onset
Spikes/s
100
0
1 sec
G_140524_8.4.a
-1000
0
1000
VLa
Mvt. onset
12
6
0
1 sec
G_140902_2.1.a
B
Response Types
100
200
300
400
Increase
Decrease
Polyphasic (+)
Polyphasic (−)
NR
10
5
0
−5
Normalized activity
-1000
1000
C
Normalized activity
Increase
All
Decrease
Polyphasic
(initial +)
Polyphasic
(initial −)
8
4
0
-4
-8
−1000
0
1000
time [relative to mvt. onset (ms)]

Fig. 3

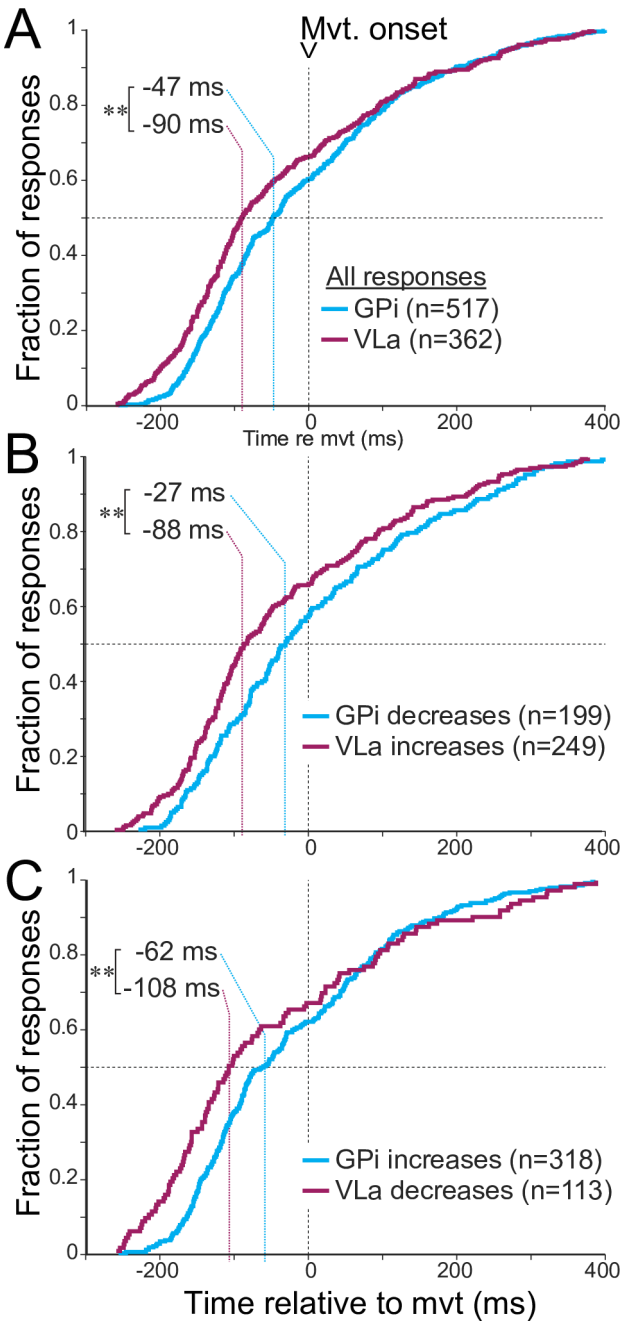
A
Mvt. onset
-47 ms
-90 ms
**
All responses
GPi (n=517)
VLa (n=362)
Fraction of responses
Time re mvt (ms)
B
-27 ms
-88 ms
**
GPi decreases (n=199)
VLa increases (n=249)
C
-62 ms
-108 ms
**
GPi increases (n=318)
VLa decreases (n=113)
Time relative to mvt (ms)

Fig. 4

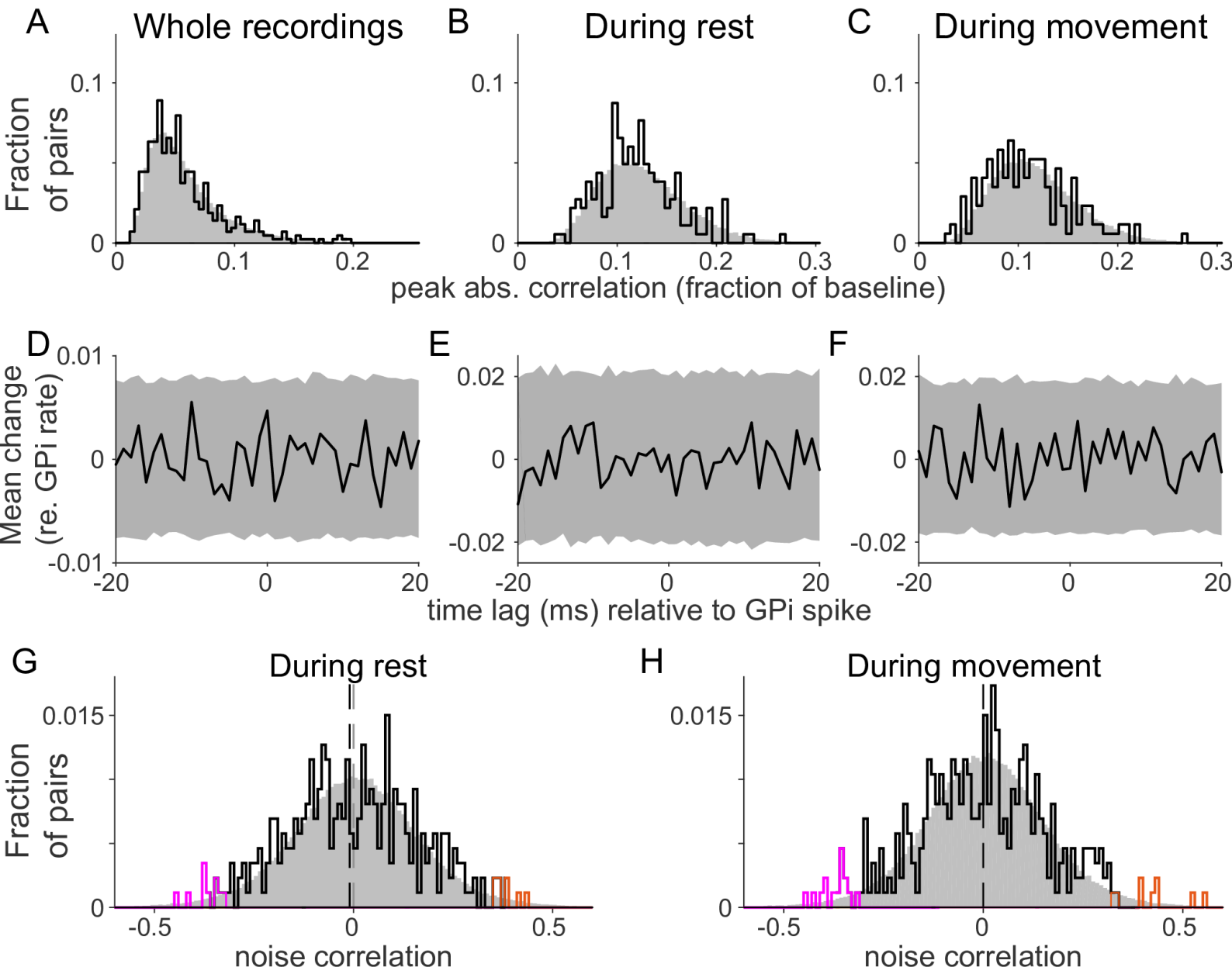
A
Whole recordings
B
During rest
C
During movement
Fraction of pairs
0.1
0
0
0.1
0.2
0.3
peak abs. correlation (fraction of baseline)
D
E
F
Mean change (re. GPi rate)
0.01
-0.01
0.02
-0.02
-20
20
time lag (ms) relative to GPi spike
G
During rest
H
During movement
0.015
-0.5
0.5
noise correlation

Fig. 5

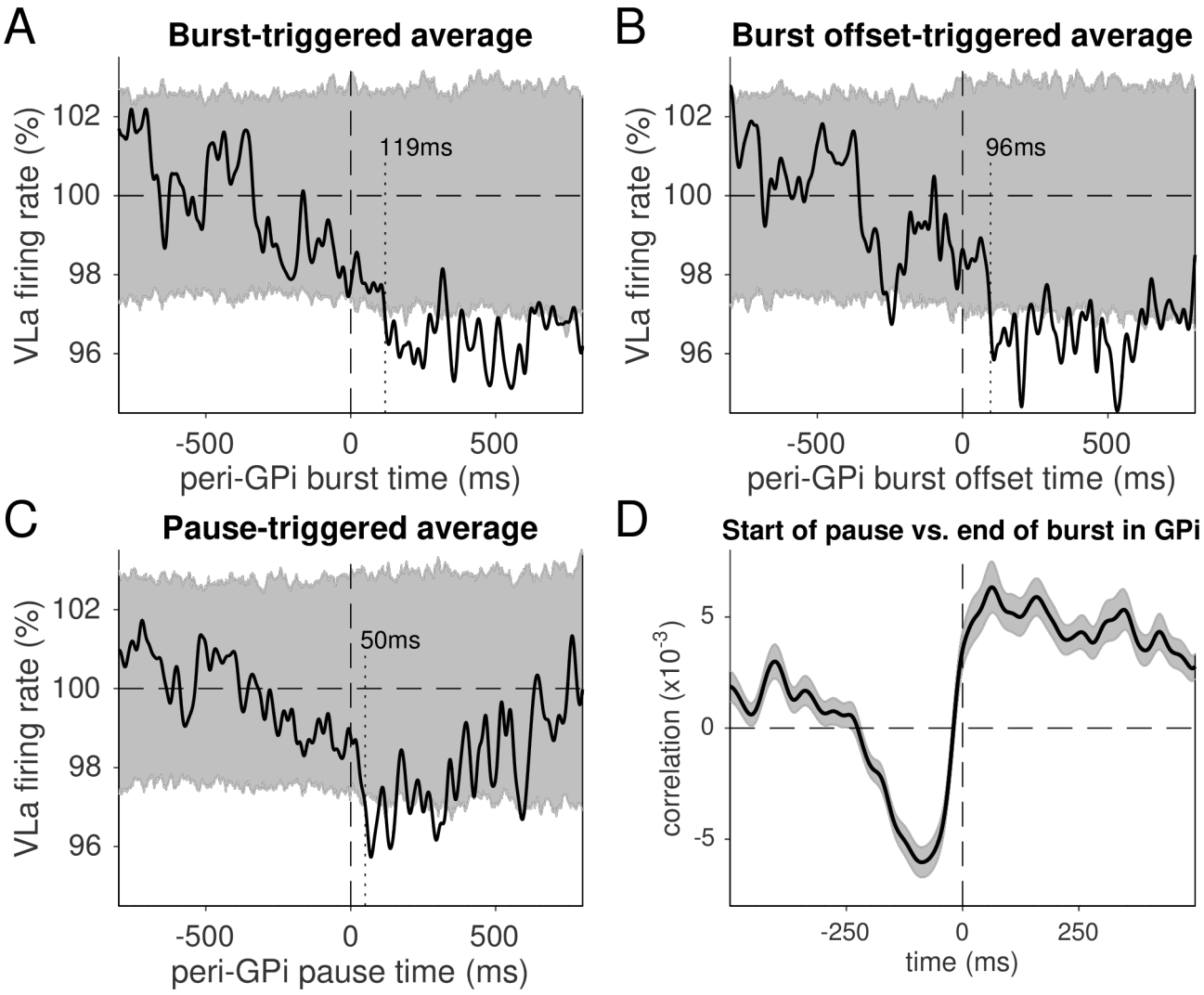
A
Burst-triggered average
VLa firing rate (%)
102
100
98
96
119ms
-500
0
500
peri-GPi burst time (ms)
B
Burst offset-triggered average
VLa firing rate (%)
102
100
98
96
96ms
-500
0
500
peri-GPi burst offset time (ms)
C
Pause-triggered average
VLa firing rate (%)
102
100
98
96
50ms
-500
0
500
peri-GPi pause time (ms)
D
Start of pause vs. end of burst in GPi
correlation (x10^{-3})
5
0
-5
-250
0
250
time (ms)

Fig. 6

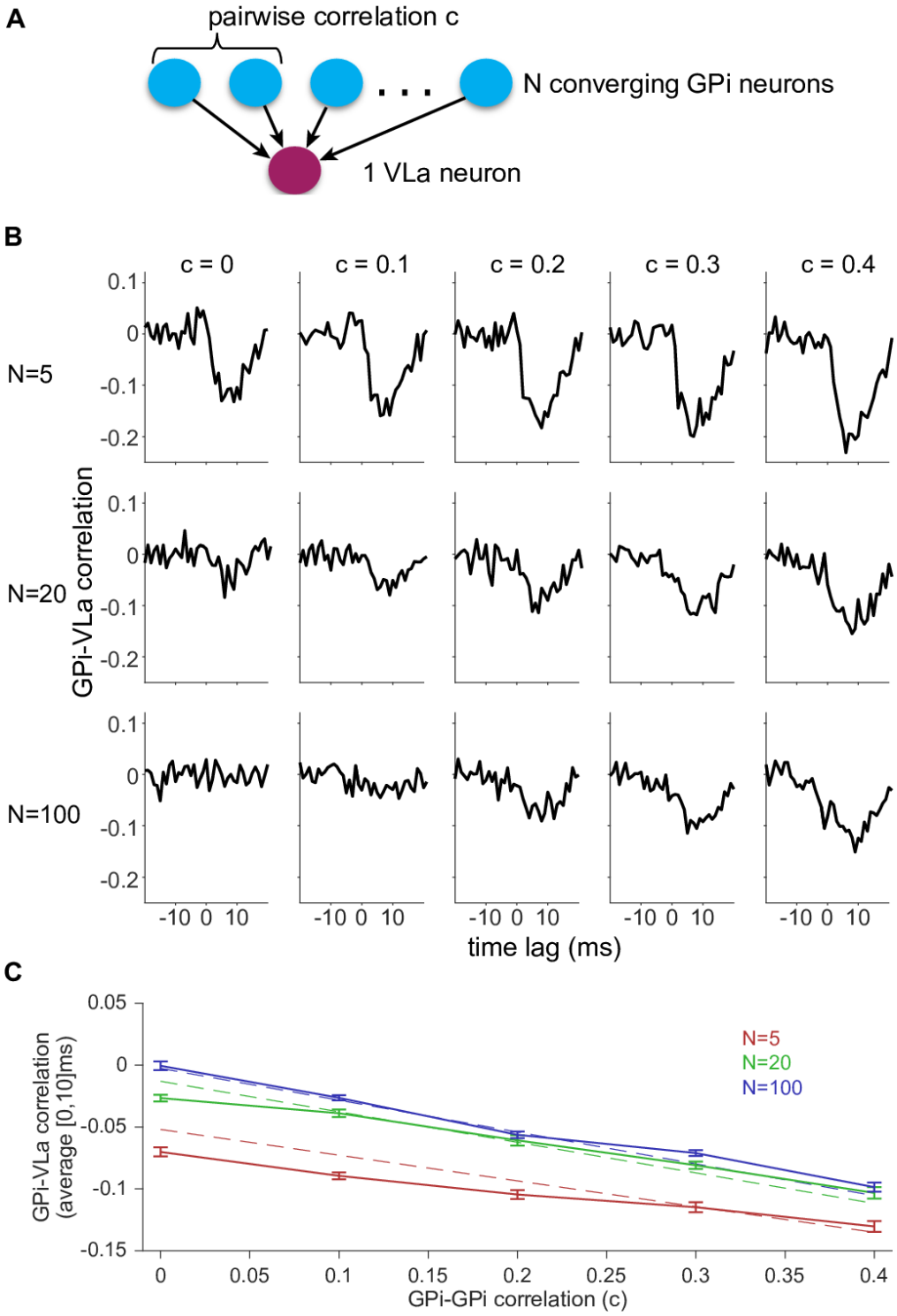
A
pairwise correlation c
N converging GPi neurons
1 VLa neuron
B
c = 0
c = 0.1
c = 0.2
c = 0.3
c = 0.4
N=5
N=20
N=100
GPi-VLa correlation
0.1
0
-0.1
-0.2
-10 0 10
time lag (ms)
C
GPi-VLa correlation (average [0,10]ms)
0.05
0
-0.05
-0.1
-0.15
N=5
N=20
N=100
0
0.05
0.1
0.15
0.2
0.25
0.3
0.35
0.4
GPi-GPi correlation (c)

Fig. S1

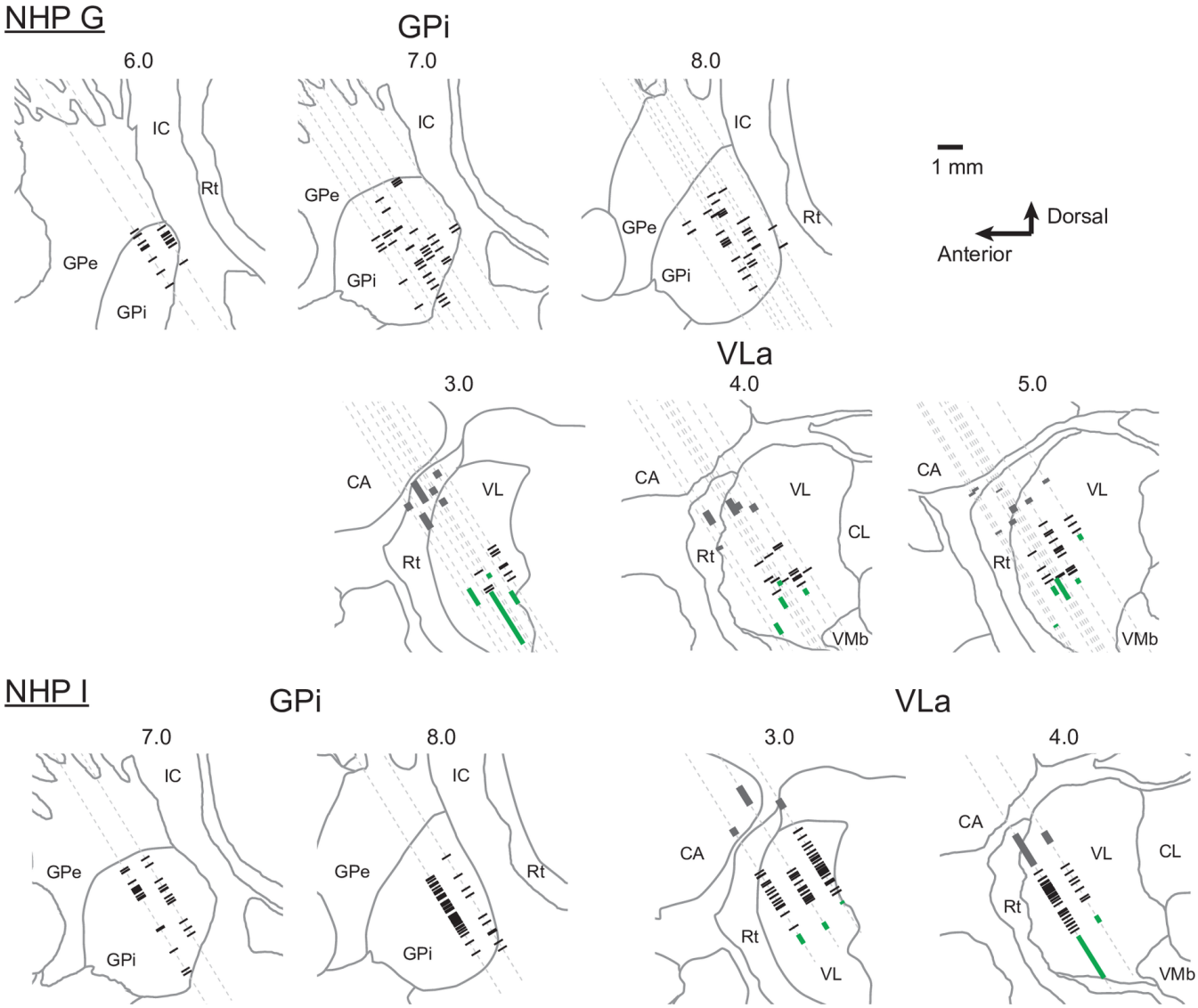
NHP G
GPi
6.0
7.0
8.0
IC
Rt
GPe
GPi
1 mm
Dorsal
Anterior
VLa
3.0
4.0
5.0
CA
VL
CL
VMb
NHP I
GPi
VLa
7.0
8.0
3.0
4.0

Fig. S2

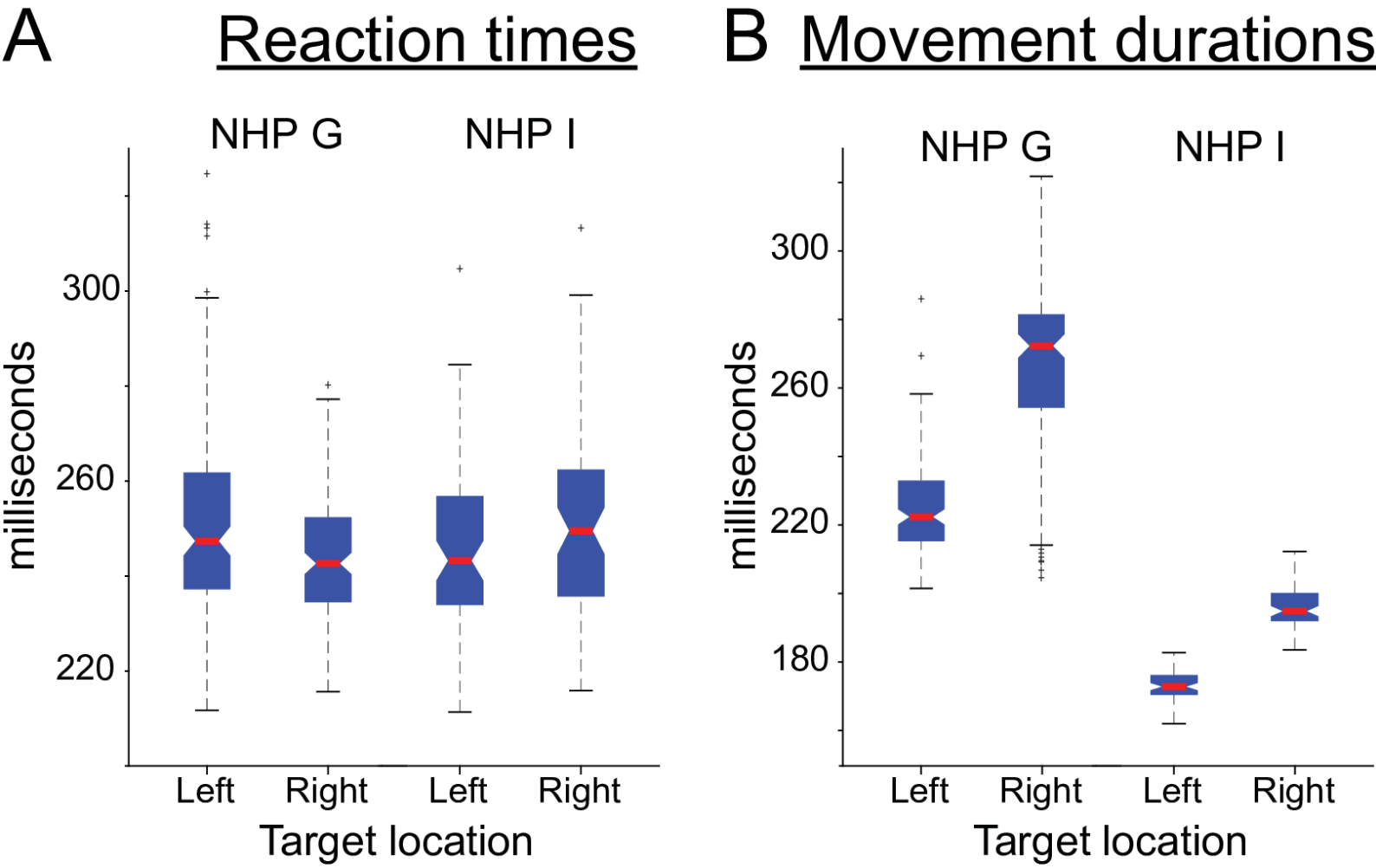
A
Reaction times
NHP G
NHP I
milliseconds
300
260
220
Left
Right
Left
Right
Target location
B
Movement durations
NHP G
NHP I
milliseconds
300
260
220
180
Left
Right
Left
Right
Target location

Fig. S3

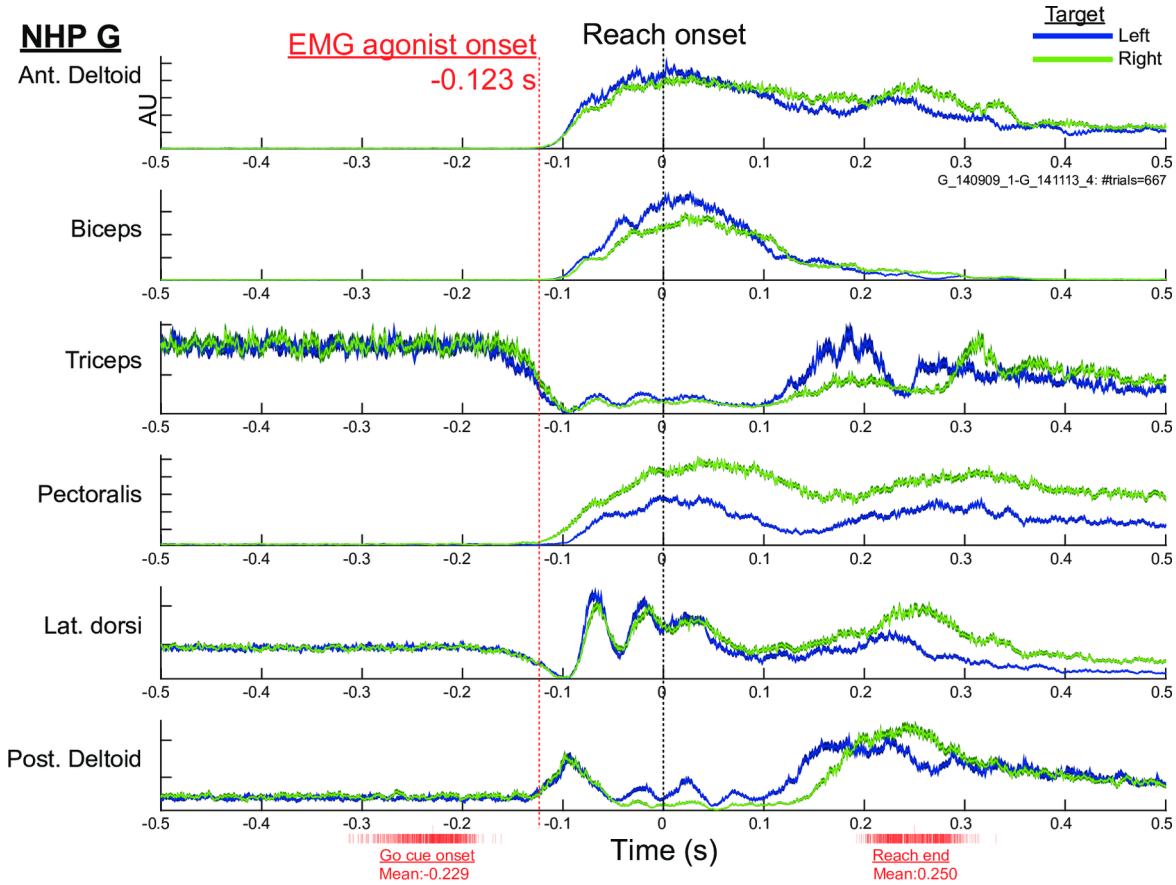
NHP G
EMG agonist onset
-0.123 s
Reach onset
Target
Left
Right
Ant. Deltoid
AU
G_140909_1-G_141113_4: #trials=667
Biceps
Triceps
Pectoralis
Lat. dorsi
Post. Deltoid
-0.5
-0.4
-0.3
-0.2
-0.1
0
0.1
0.2
0.3
0.4
0.5
Go cue onset
Mean:-0.229
Time (s)
Reach end
Mean:0.250

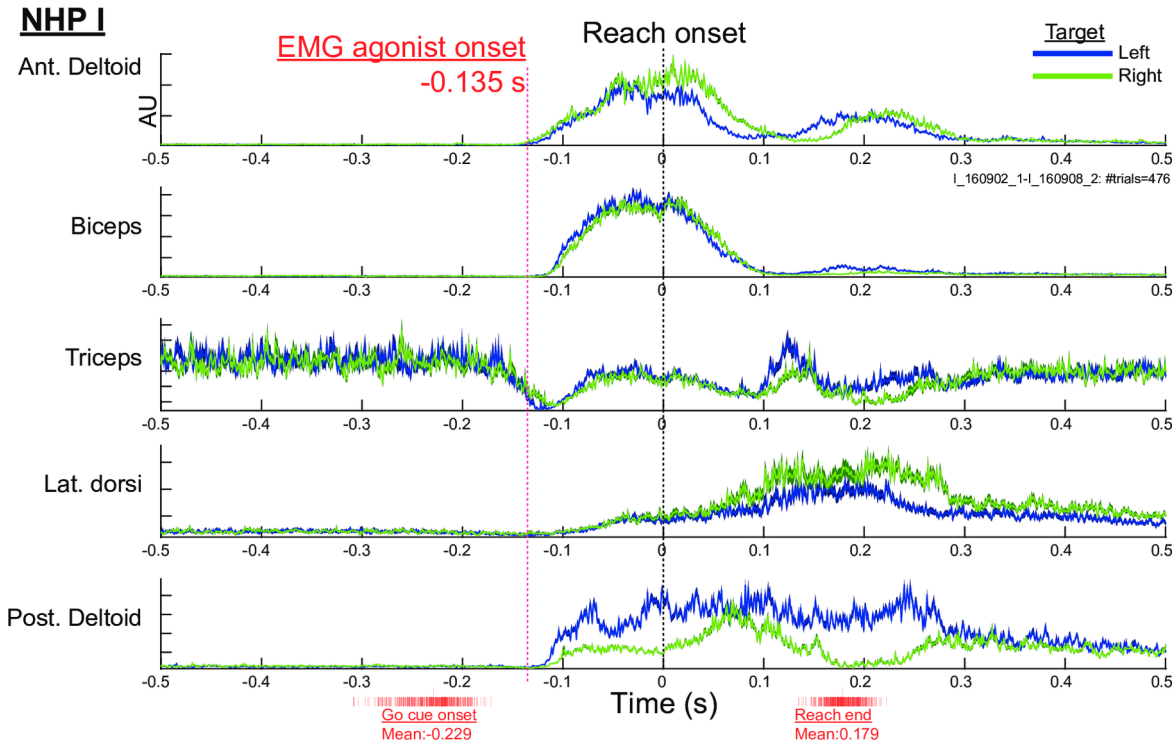
NHP I
EMG agonist onset
-0.135 s
Reach onset
Target
Left
Right
Ant. Deltoid
AU
I_160902_1-I_160908_2: #trials=476
Biceps
Triceps
Lat. dorsi
Post. Deltoid
-0.5
-0.4
-0.3
-0.2
-0.1
0
0.1
0.2
0.3
0.4
0.5
Go cue onset
Mean:-0.229
Time (s)
Reach end
Mean:0.179

Fig. S4

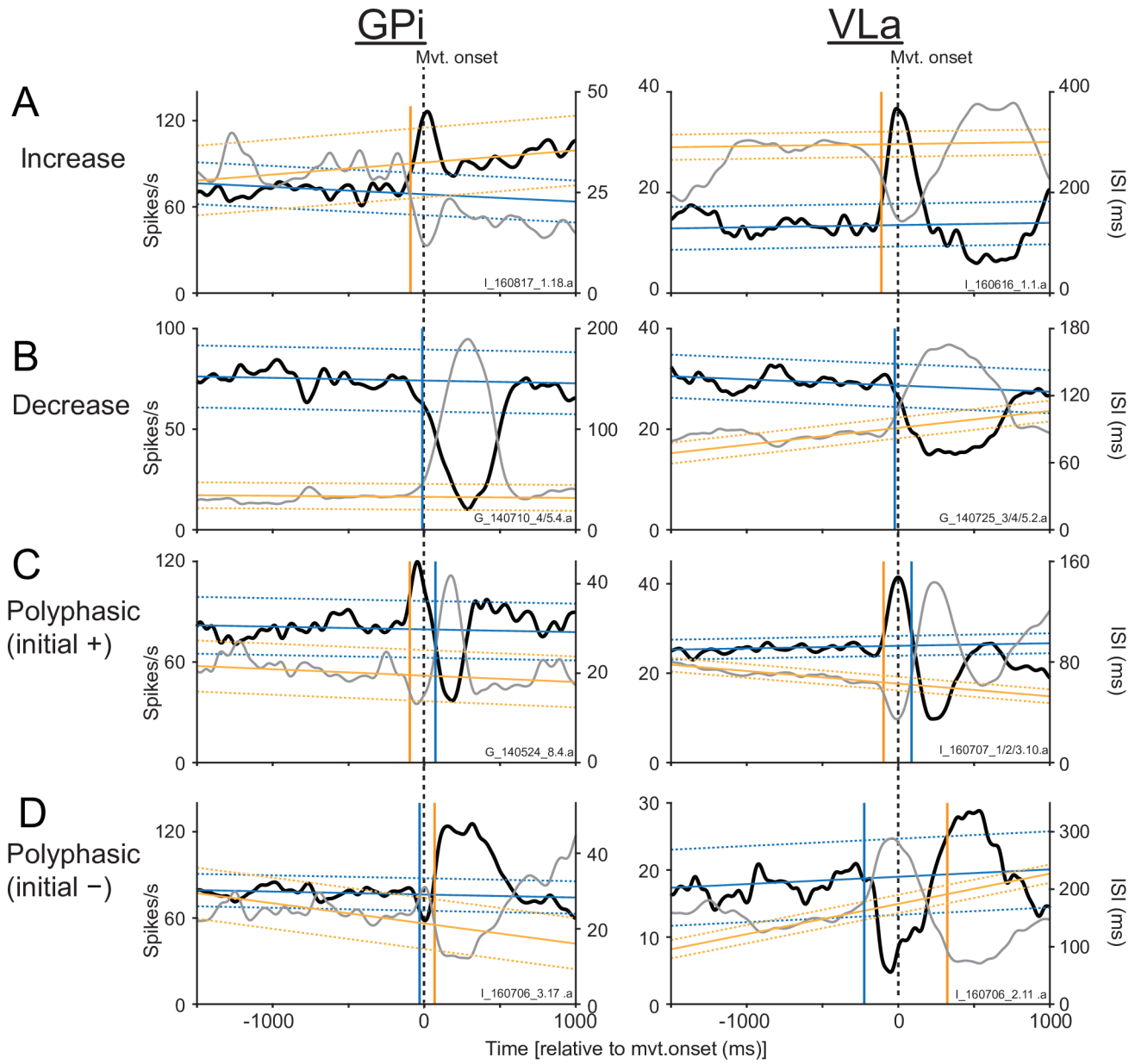
GPi
VLa
Mvt. onset
Mvt. onset
A
Increase
B
Decrease
C
Polyphasic
(initial +)
D
Polyphasic
(initial −)
Spikes/s
ISI (ms)
I_160817_1.18.a
I_160616_1.1.a
G_140710_4/5.4.a
G_140725_3/4/5.2.a
G_140524_8.4.a
I_160707_1/2/3.10.a
I_160706_3.17 .a
I_160706_2.11 .a
-1000
0
1000
Time [relative to mvt.onset (ms)]

Fig. S5

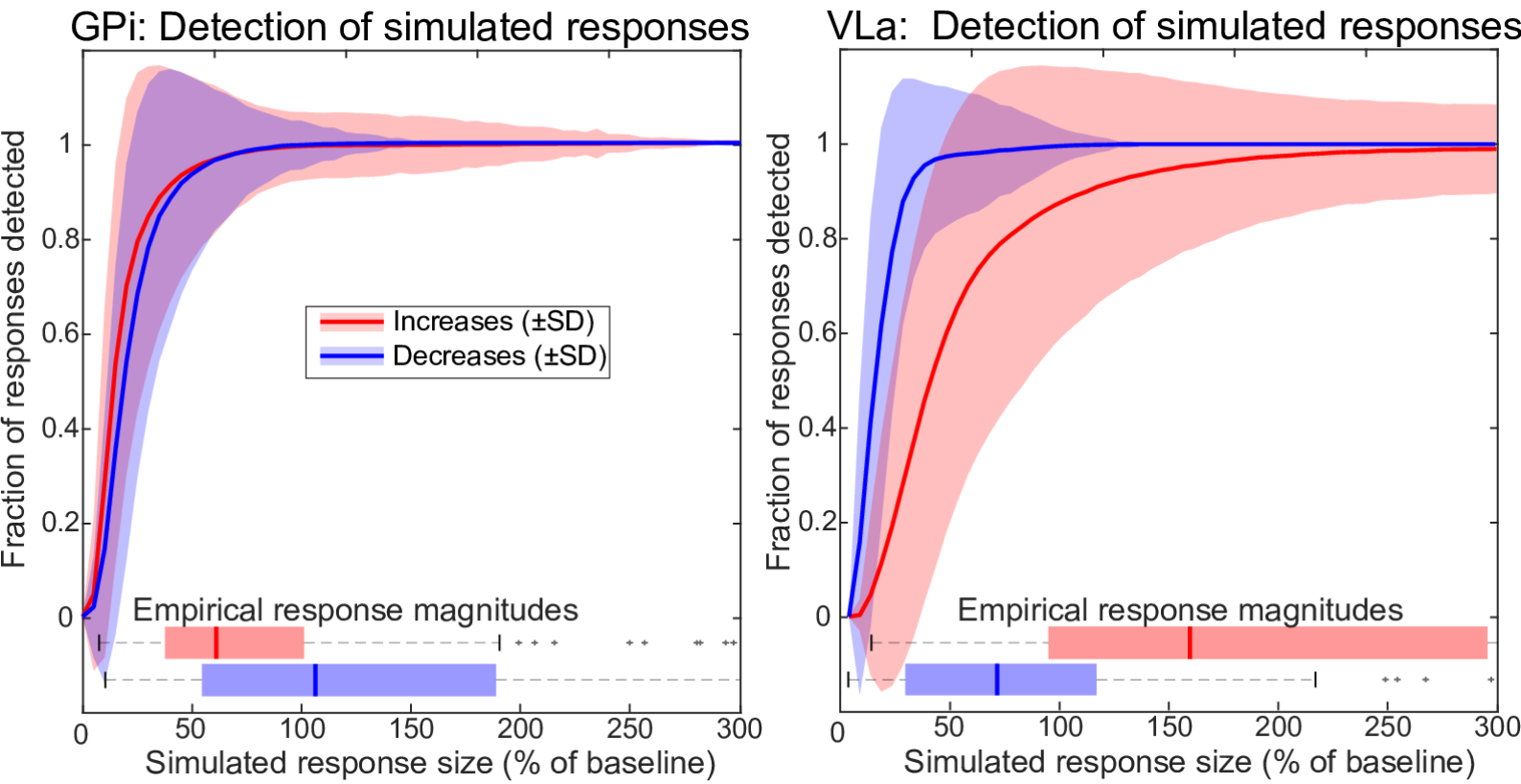
GPi: Detection of simulated responses
VLa: Detection of simulated responses
Fraction of responses detected
Simulated response size (% of baseline)
Increases (±SD)
Decreases (±SD)
Empirical response magnitudes
0
0.2
0.4
0.6
0.8
1
0
50
100
150
200
250
300

Fig. S6

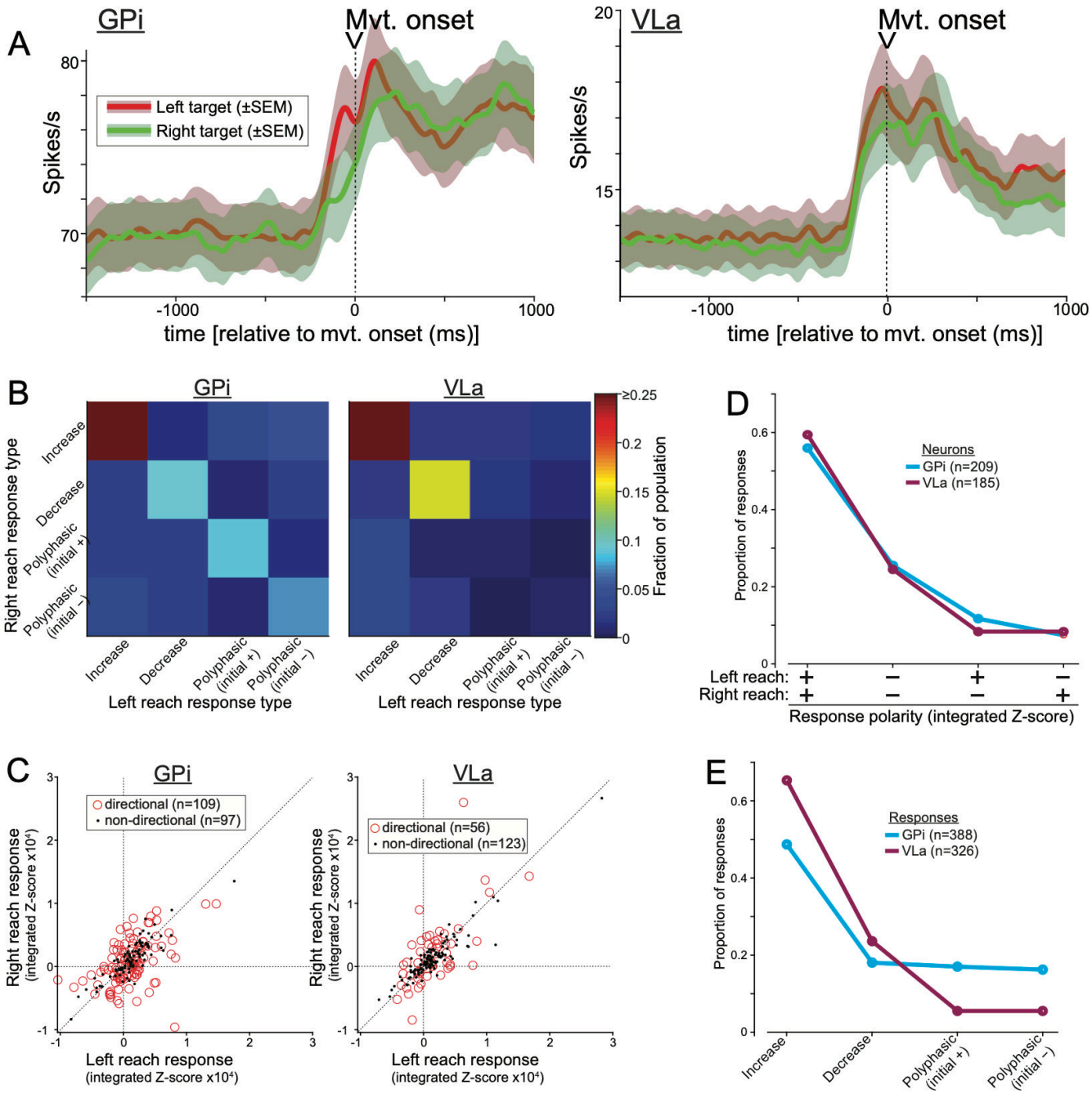
A
GPi
Mvt. onset
Left target (±SEM)
Right target (±SEM)
Spikes/s
time [relative to mvt. onset (ms)]
VLa
Mvt. onset
Spikes/s
time [relative to mvt. onset (ms)]
B
GPi
VLa
Right reach response type
Increase
Decrease
Polyphasic (initial +)
Polyphasic (initial −)
Left reach response type
Fraction of population
D
Neurons
GPi (n=209)
VLa (n=185)
Proportion of responses
Left reach:
Right reach:
Response polarity (integrated Z-score)
C
GPi
directional (n=109)
non-directional (n=97)
VLa
directional (n=56)
non-directional (n=123)
Right reach response (integrated Z-score x10⁴)
Left reach response (integrated Z-score x10⁴)
E
Responses
GPi (n=388)
VLa (n=326)
Proportion of responses
Increase
Decrease
Polyphasic (initial +)
Polyphasic (initial −)

Fig. S7

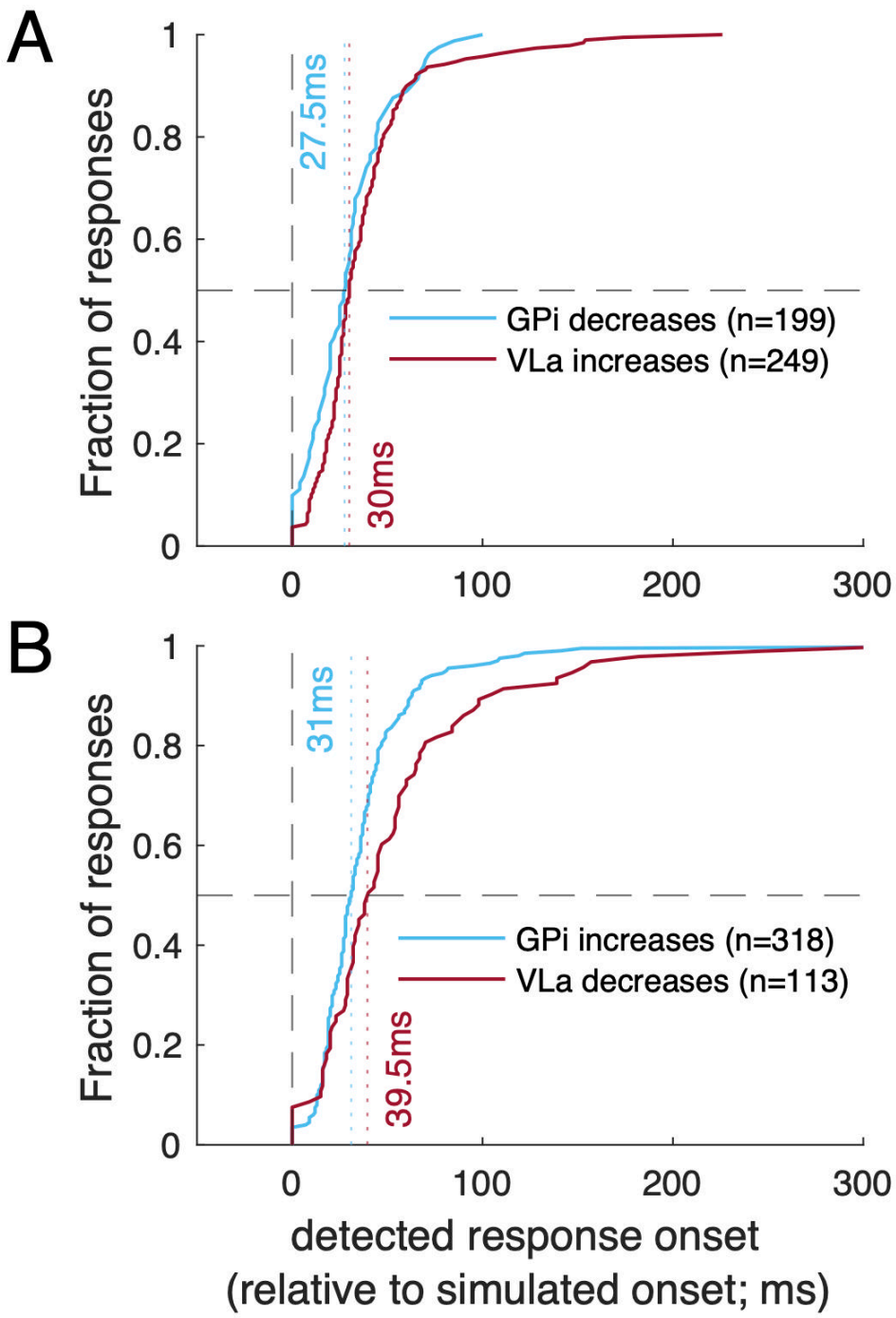
A
Fraction of responses
1
0.8
0.6
0.4
0.2
0
27.5ms
30ms
GPi decreases (n=199)
VLa increases (n=249)
0
100
200
300
B
Fraction of responses
1
0.8
0.6
0.4
0.2
0
31ms
39.5ms
GPi increases (n=318)
VLa decreases (n=113)
0
100
200
300
detected response onset
(relative to simulated onset; ms)

Fig. S8

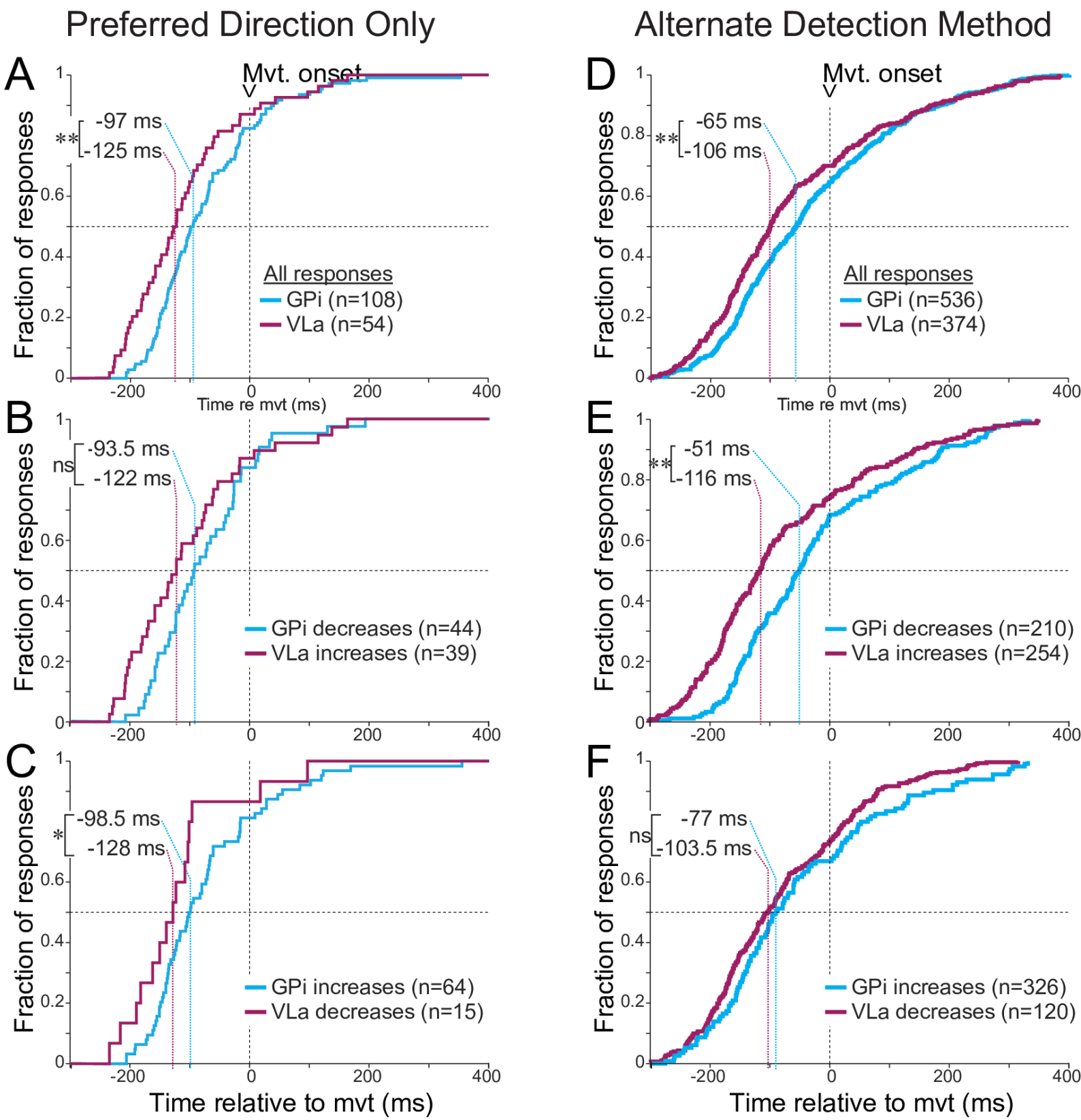
Preferred Direction Only
Alternate Detection Method
A
Mvt. onset
-97 ms
-125 ms
**
All responses
GPi (n=108)
VLa (n=54)
Fraction of responses
Time re mvt (ms)
B
-93.5 ms
-122 ms
ns
GPi decreases (n=44)
VLa increases (n=39)
C
-98.5 ms
-128 ms
*
GPi increases (n=64)
VLa decreases (n=15)
Time relative to mvt (ms)
D
Mvt. onset
-65 ms
-106 ms
**
All responses
GPi (n=536)
VLa (n=374)
E
-51 ms
-116 ms
**
GPi decreases (n=210)
VLa increases (n=254)
F
-77 ms
-103.5 ms
ns
GPi increases (n=326)
VLa decreases (n=120)
Time relative to mvt (ms)

Fig. S9

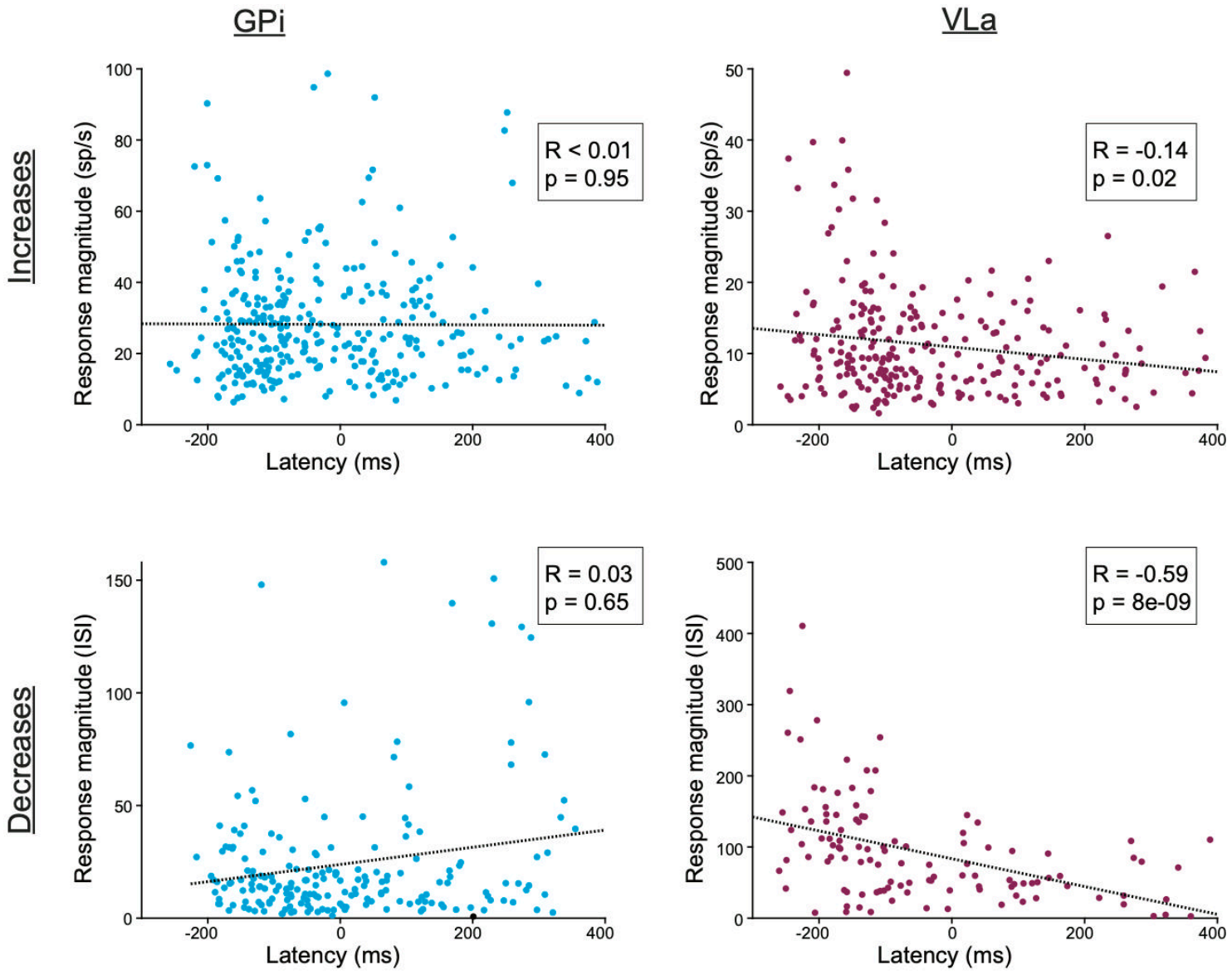
GPi
VLa
Increases
Decreases
Response magnitude (sp/s)
Response magnitude (ISI)
Latency (ms)
R < 0.01
p = 0.95
R = -0.14
p = 0.02
R = 0.03
p = 0.65
R = -0.59
p = 8e-09

Fig. S10

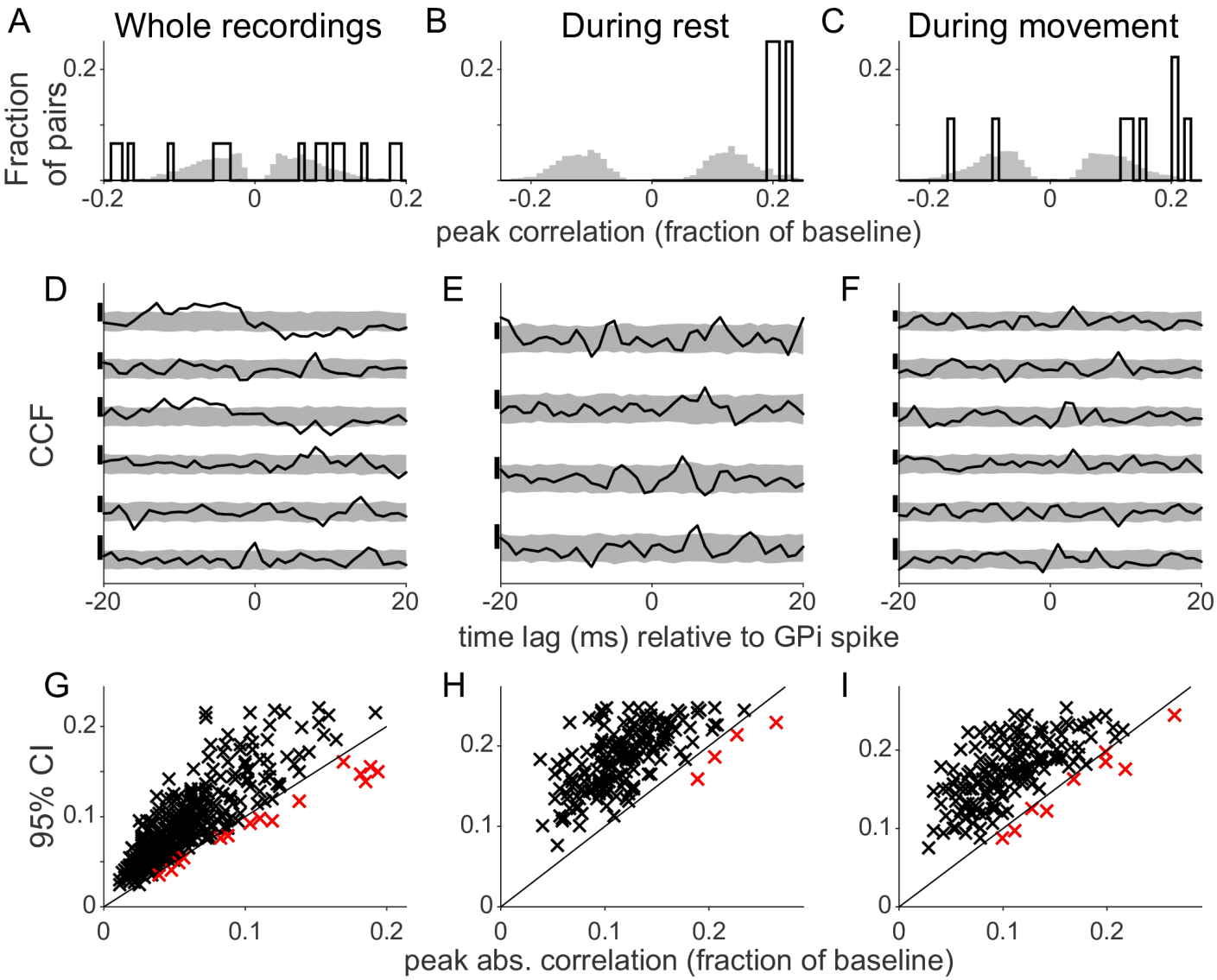
A
Whole recordings
B
During rest
C
During movement
Fraction of pairs
0.2
-0.2
0
0.2
peak correlation (fraction of baseline)
D
E
F
CCF
-20
0
20
time lag (ms) relative to GPi spike
G
H
I
95% CI
0.2
0.1
0
0.1
0.2
peak abs. correlation (fraction of baseline)

Fig. S11

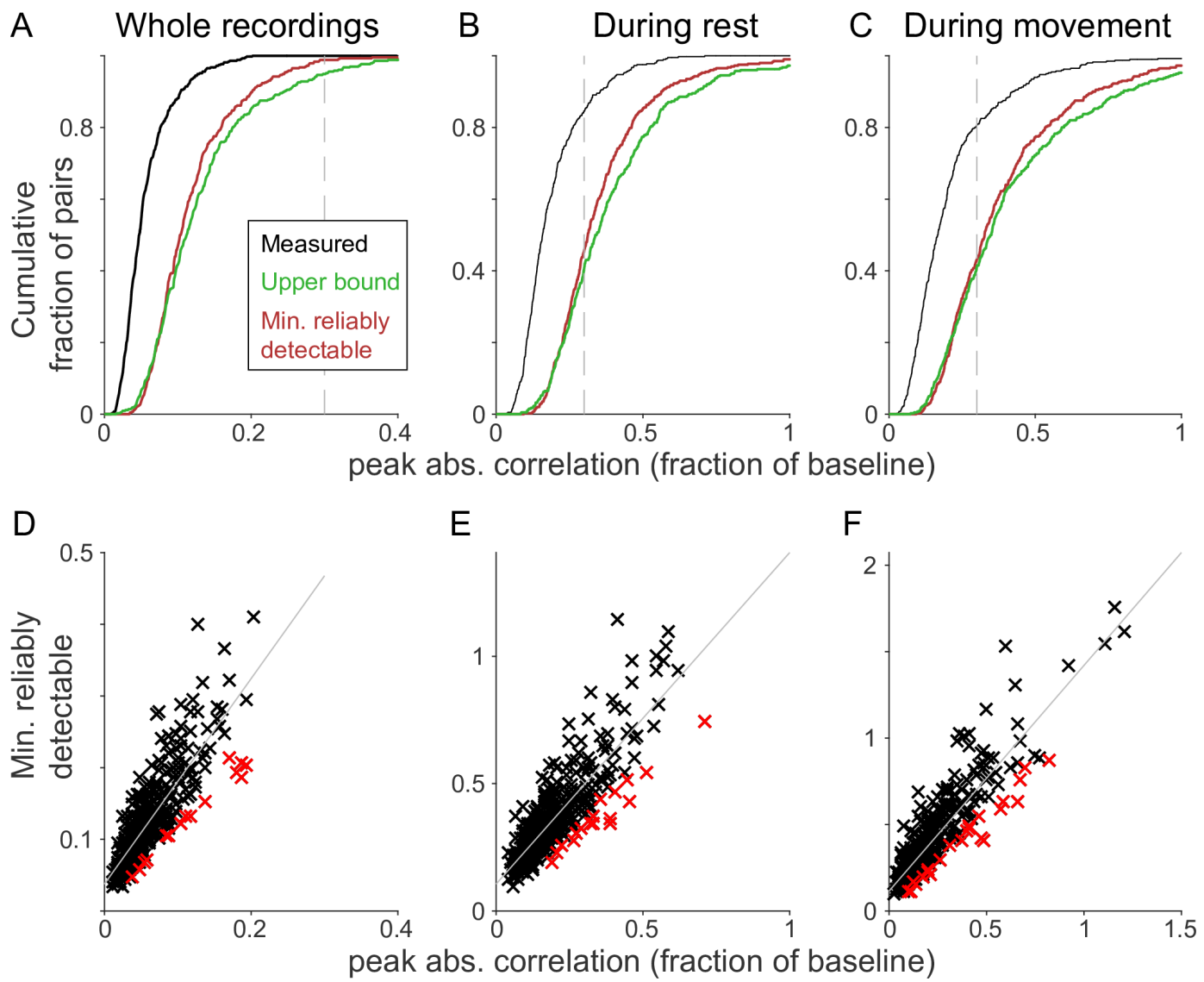
A
Whole recordings
B
During rest
C
During movement
Cumulative fraction of pairs
Measured
Upper bound
Min. reliably detectable
peak abs. correlation (fraction of baseline)
D
E
F
Min. reliably detectable
peak abs. correlation (fraction of baseline)

Fig. S12

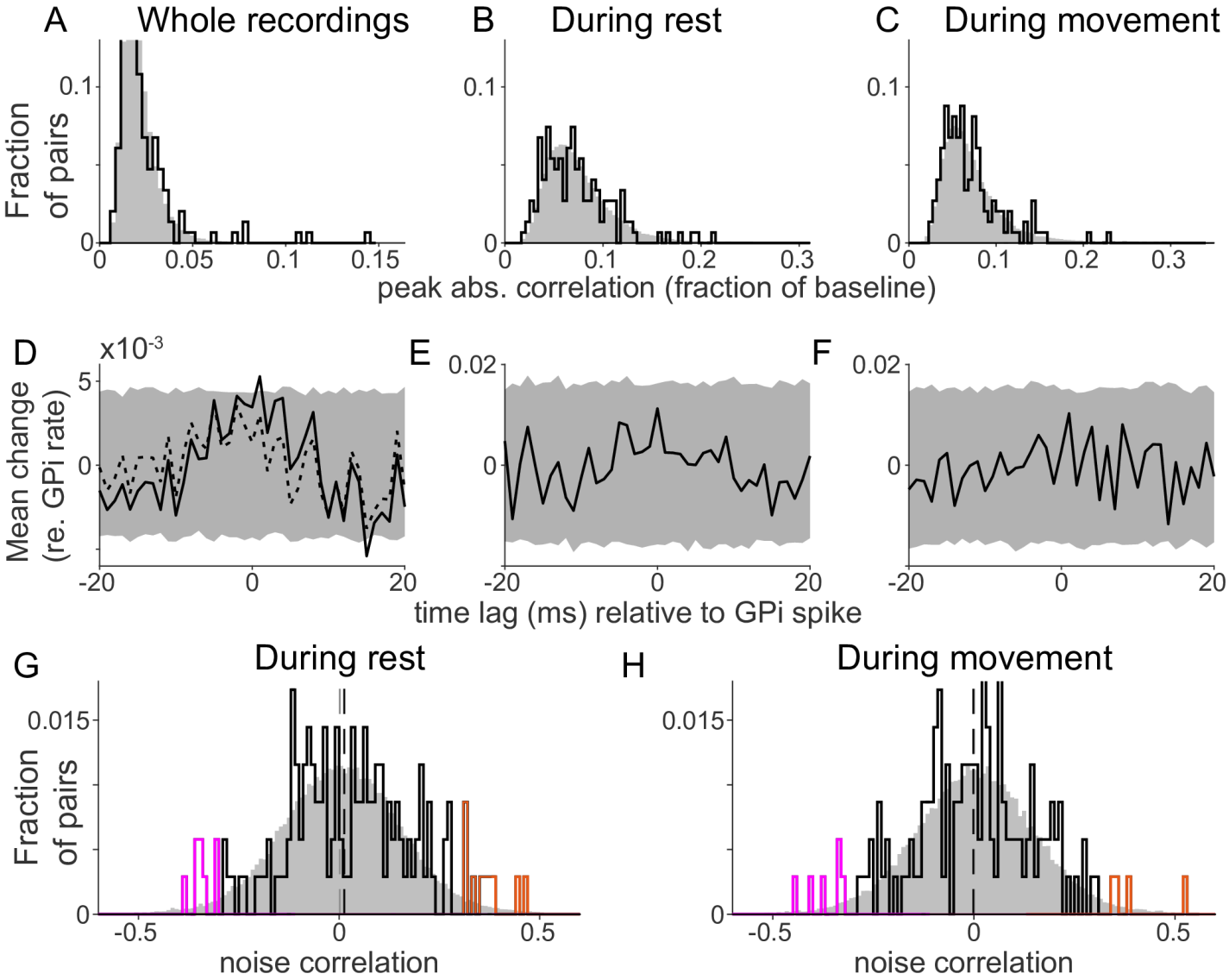
A
Whole recordings
B
During rest
C
During movement
Fraction of pairs
0.1
0
0
0.05
0.1
0.15
0
0.1
0.2
0.3
peak abs. correlation (fraction of baseline)
D
x10-3
5
0
E
0.02
F
Mean change (re. GPi rate)
-20
20
time lag (ms) relative to GPi spike
G
During rest
H
During movement
0.015
-0.5
0.5
noise correlation

Fig. S13

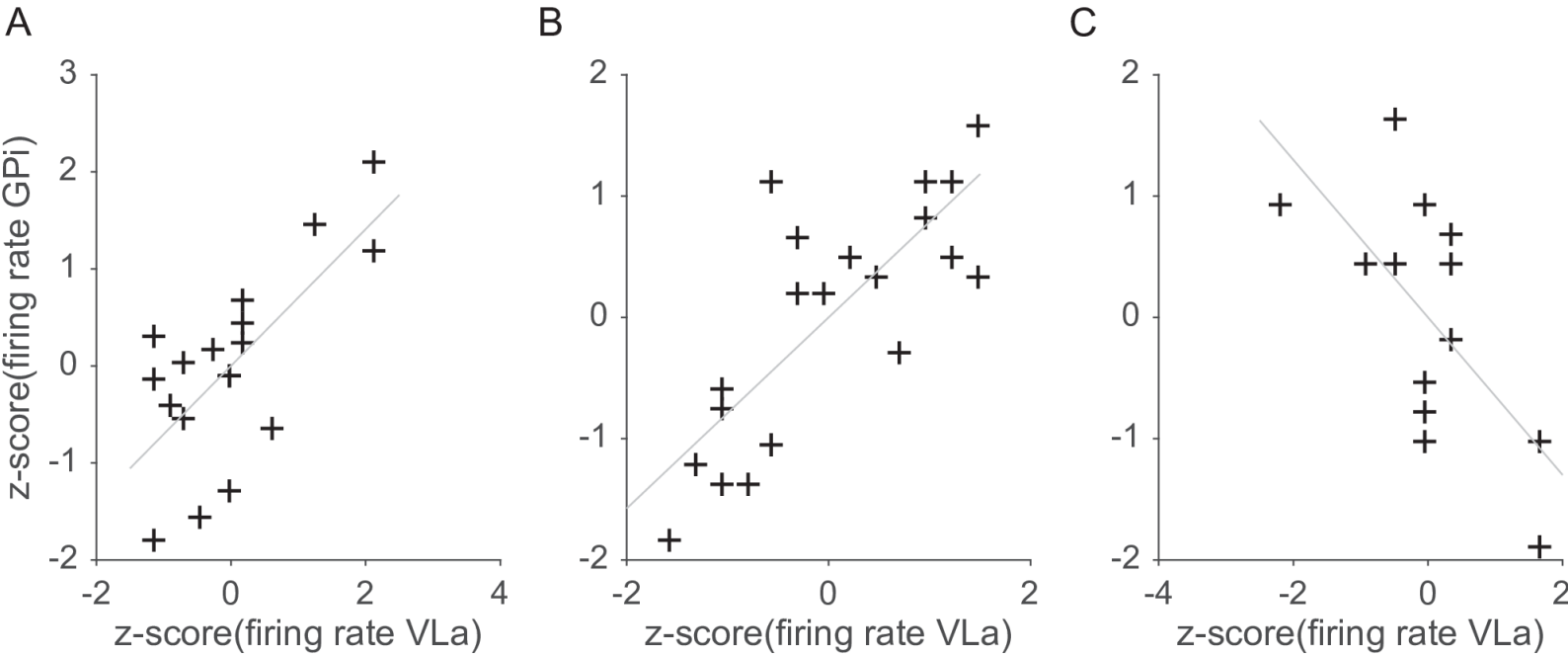
A
B
C
z-score(firing rate GPi)
z-score(firing rate VLa)
z-score(firing rate VLa)
z-score(firing rate VLa)
3
2
1
0
-1
-2
-2
0
2
4
2
1
0
-1
-2
-2
0
2
2
1
0
-1
-2
-4
-2
0
2

Fig. S14

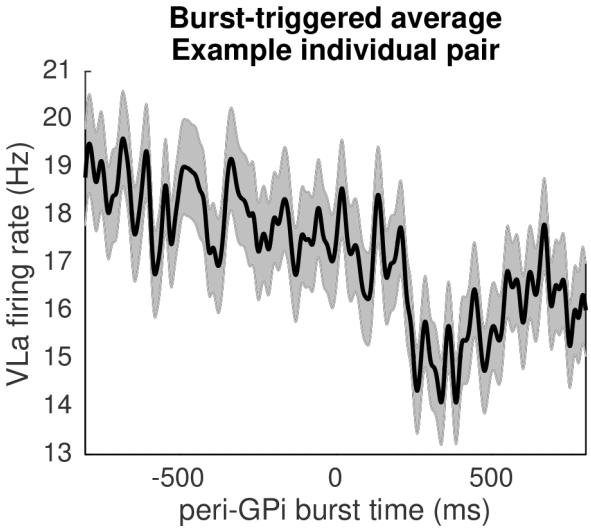
Burst-triggered average
Example individual pair
VLa firing rate (Hz)
21
20
19
18
17
16
15
14
13
-500
0
500
peri-GPi burst time (ms)